





Title	Metabolomic characterization of monoclonal antibody-producing Chinese hamster lung (CHL)-YN cells in glucose-controlled serum-free fed-batch operation
Author(s)	Sukwattananipaat, Puriwat; Kuroda, Hirotaka; Yamano-Adachi, Noriko et al.
Citation	Biotechnology and Bioengineering. 2024
Version Type	VoR
URL	https://hdl.handle.net/11094/97616
rights	This article is licensed under a Creative Commons Attribution 4.0 International License.
Note	

Osaka University Knowledge Archive : OUKA

<https://ir.library.osaka-u.ac.jp/>

Osaka University

Metabolomic characterization of monoclonal antibody-producing Chinese hamster lung (CHL)-YN cells in glucose-controlled serum-free fed-batch operation

Puriwat Sukwattananipaat¹  | Hirotaka Kuroda^{1,2,3}  |
Noriko Yamano-Adachi^{1,4,5}  | Takeshi Omasa^{1,4,5} 

¹Graduate School of Engineering, Osaka University, Osaka, Japan

²Shimadzu Corp., Kyoto, Japan

³Shimadzu Analytical Innovation Research Laboratories, Osaka, Japan

⁴Institute for Open and Transdisciplinary Research Initiatives, Osaka University, Osaka, Japan

⁵Manufacturing Technology Association of Biologics (MAB), Hyogo, Japan

Correspondence

Noriko Yamano-Adachi, Graduate School of Engineering, Osaka University, 2-1 Yamadaoka, Suita, Osaka 565-0871, Japan.
Email: yamanori@bio.eng.osaka-u.ac.jp

Funding information

Nikki/Saneyoshi Scholarship; Japan Agency for Medical Research and Development (AMED), Grant/Award Numbers: JP18ae0101066, JP21ae0121021; Japan Society for the Promotion of Science (JSPS), Grant/Award Numbers: JP21K04788, JP22H00276; Kinoshita Memorial Foundation Scholarship Program

Abstract

The fast-growing Chinese hamster lung (CHL)-YN cell line was recently developed for monoclonal antibody production. In this study, we applied a serum-free fed-batch cultivation process to immunoglobulin (Ig)G1-producing CHL-YN cells, which were then used to design a dynamic glucose supply system to stabilize the extracellular glucose concentration based on glucose consumption. Glucose consumption of the cultures rapidly oscillated following three phases of glutamine metabolism: consumption, production, and re-consumption. Use of the dynamic glucose supply prolonged the viability of the CHL-YN-IgG1 cell cultures and increased IgG1 production. Liquid chromatography with tandem mass spectrometry-based target metabolomics analysis of the extracellular metabolites during the first glutamine shift was conducted to search for depleted compounds. The results suggest that the levels of four amino acids, namely arginine, aspartate, methionine, and serine, were sharply decreased in CHL-YN cells during glutamine production. Supporting evidence from metabolic and gene expression analyses also suggest that CHL-YN cells acquired ornithine- and cystathionine-production abilities that differed from those in Chinese hamster ovary-K1 cells, potentially leading to proline and cysteine biosynthesis.

KEYWORDS

Chinese hamster lung, CHL-YN cells, CHO cells, fed-batch, glucose feeding development, metabolomics

1 | INTRODUCTION

Monoclonal antibodies (mAbs) are recombinant therapeutic proteins whose market value has grown continuously since 2002 (Lu et al., 2020) and now represents the largest portion of sales in the biopharmaceutical market. In 2021, mAbs reportedly comprised over

80% of total biopharmaceutical substances sold (Walsh & Walsh, 2022). Amid the rising demand for mAbs, several bioprocess strategies have been developed under competitive market pressure. For instance, use of efficient expression vector design, high-throughput technologies, and automation devices are all aimed at reducing production time (Agrawal & Bal, 2012). Recently, the

This is an open access article under the terms of the [Creative Commons Attribution](https://creativecommons.org/licenses/by/4.0/) License, which permits use, distribution and reproduction in any medium, provided the original work is properly cited.

© 2024 The Author(s). *Biotechnology and Bioengineering* published by Wiley Periodicals LLC.

strategy of novel cell line construction has produced cell lines with unique properties compared with the original expression hosts. These include: Chinese hamster ovary (CHO)-MK cells, a next-generation CHO cell line that quickly produces high levels of mAbs; Chinese hamster lung (CHL)-YN cells, a fast-growing cell line with reportedly high expression of glutamine synthetase; and Chinese hamster kidney (CHK)-Q cells, a kidney-derived immortalized cell line with potential as a therapeutic protein host expression system and a renal stem cell model (Horiuchi, 2019; Kawabe & Kamihira, 2022; Okamura et al., 2022; Yamano-Adachi et al., 2020).

Currently, the dominant expression host used for industrial mAb bioprocessing is the CHO cell (Kunert & Reinhart, 2016; Tihanyi & Nyitray, 2020; Walsh & Walsh, 2022). This ovarian epithelial-derived cell line was originated by Dr. Theodore T. Puck, who isolated the immortalized cell pool from a Chinese hamster (*Cricetulus griseus*) in 1957 (Puck et al., 1958; Wurm & Hacker, 2011). CHO cell lines are widely used because of their attractive attributes, including protein modification and glycosylation, invulnerability to several human pathogenic viruses, serum-free adaptation, and scale-up capabilities (Berting et al., 2010; Omasa et al., 2010). Nevertheless, CHO cell cultures are limited by a slow growth rate compared with nonmammalian expression hosts, such as *Escherichia coli*, *Saccharomyces cerevisiae*, and *Pichia pastoris* (Horie et al., 2022). Torpid growth protracts stable cell pool construction, resulting in a time-consuming, resource-intensive cell line development process (Poulain et al., 2019).

CHL-YN (RIKEN Bioresource Cell Bank, RCB5004), newly isolated and cultivated by Yamano-Adachi et al. (2020), is a lung fibroblast-derived cell line that has similar properties to CHO cells in terms of glycosylation profile and cell culture performance. Remarkably, CHL-YN cells feature an approximately twofold faster growth rate and higher expression of glutamine synthetase mRNA compared with CHO-K1 cells. Therefore, CHL-YN has potential for development as an alternative expression host for mAb production.

In industrial mAb production, serum-free fed-batch cultivation is commonly selected for routine culturing of the mAb-expressing host because of the simplicity of facility requirements and efficiency of production (Fan et al., 2018; Ritacco et al., 2018). Furthermore, fed-batch cultivation with intensified cell concentrations is performed using a high cell seed train, usually prepared by an N-1 perfusion strategy called process intensification, which has recently been employed to raise mAb production up to 3.5–4.5 g/L (Schulze et al., 2022; Stepper et al., 2020). Hence, serum-free fed-batch culture was applied and developed in the mAb-producing CHL-YN cell line. Beyond the conventional fed-batch scheme, a dynamic glucose feed control system was designed for CHL-YN cell cultivation to avoid excessive glucose levels. The dynamic glucose feed strategy modified the fed-glucose volumes depending on cell-specific glucose consumption rates, which dynamically shift during cultivation. Excessive glucose in cell cultures leads to abundant lactate accumulation and is detrimental to cell growth (Lee et al., 2015).

Exploring the nutrients and intermediates that become limited during the cell cultivation process and critically affect cell

survivability and productivity in the late stage is also key to improving cell culture performance (Pereira et al., 2018). Metabolomics is a tool to comprehensively investigate the biochemical compounds in biological systems, including mammalian cell lines (Čuperlović-Culf et al., 2010; Stolfa et al., 2018; Zhang & Ramautar, 2021). Several studies have used metabolomics to identify the exclusive metabolic contents of CHO cell lines cultured under various conditions to better understand their physiological properties. For instance, studies have described metabolic compound dissimilarities between high and low mAb-producing CHO clones (Chong et al., 2012), distinct stress-response metabolites produced under different stress conditions (Badsha et al., 2016), and differences in metabolic data sets among the four phases of CHO growth (Vodopivec et al., 2019). However, such studies have not been conducted on the CHL-YN cell line. Gathering knowledge about the CHL-YN metabolic background is an important step toward developing suitable CHL-YN cell cultivation methodologies based on physiological preferences.

In this study, we first developed a glucose feed strategy for a new fast-growing cell line, mAb-producing CHL-YN, using a serum-free fed-batch culture process to maintain the glucose concentration at a low level. Then, we investigated the extracellular and intracellular metabolites involved in central energy-associated pathways via targeted metabolomics profiling approach. Using metabolomics analysis, we aimed to search for critical limited compounds during the cultivation of mAb-producing CHL-YN cells. Furthermore, we compared the content of these compounds between CHL-YN and CHO-K1 cells to explore potential differences in their metabolic backgrounds. Understanding the CHL-YN cell characteristics could light the way to improve mAb-producing CHL-YN cell culture performance.

2 | MATERIALS AND METHODS

2.1 | Cell lines, cultures, and clone isolation

Recombinant immunoglobulin (Ig)G1 (trastuzumab)-producing CHL-YN and CHO-K1 suspension cell lines were established by polyethyleneimine-based transfection using a previously described puromycin-based selection method (Yamano-Adachi et al., 2020). The CHL-YN B-08 cell clone, which had the highest IgG expression among the 17 clones that were isolated, was derived from limiting dilution of the CHL-YN-IgG1 cell pool after transfection and selection. All cell lines were cultivated in serum-free chemically defined EX-CELL[®] CD CHO Fusion medium (Merck) supplemented with 6 mM L-Glutamine (FUJIFILM Wako Pure Chemical) and 5 µg/mL Puromycin (Invivogen). All flask-scale cultures were incubated in a Climo-shaker ISFI-X incubator (Kühner) at 37.0°C, 5% CO₂ gas, 80% humidity, and a 90 rpm rotation speed. Puromycin was continuously supplied, in accordance with a previous study (Yamano-Adachi et al., 2020). Puromycin at 5 µg/mL was added with the aim of restricting the growth of non-antibody-producing cells that had lost the antibody-expressing gene cassettes during the subsequent cultivations. Under

these conditions, no negative effects on the growth and productivity of IgG1-producing CHL-YN and CHO-K1 cells were observed.

2.2 | Bioreactor serum-free fed-batch cultivation

Both the cell pool and B-08 clone of the CHL-YN-IgG1 cell line and the CHO-K1-IgG1 cell pool were cultured in a Yokogawa BR1000 stirred-tank bioreactor (Yokogawa Electric). All cell lines were cultivated in a series of flasks to scale-up for inoculation of the 2-L bioreactor. The CHL-YN-IgG1 cell pool and B-08 clone were seeded at the viable cell concentration of 0.1×10^6 cells/mL, whereas the CHO-K1-IgG1 cell pool was seeded at 0.5×10^6 cells/mL in the serum-free fed-batch operation. EX-CELL[®] Advanced CHO fed-batch medium (Merck) supplemented with 6 mM L-glutamine, 5 µg/mL puromycin, 100 U/mL penicillin, and 100 µg/mL streptomycin (Thermo Fisher Scientific) was used as the basal medium. The control system culture conditions were set to 7.17–7.22 pH, 37.0°C temperature, 80–180 rpm cascade agitation, and 50% saturated dissolved oxygen. Feeding was performed continuously using a feed medium, EX-CELL[®] Advanced CHO Feed 1 without glucose and glutamine (Merck) and 30% D (+)-glucose solution (FUJIFILM Wako Pure Chemical), with separate feed lines. EX-CELL[®] Advanced CHO Feed 1 was continuously fed in a constant volume at 2.5% of the initial working volume per day (50 mL/day) from Day 2 of cultivation onward in all cultivations. Increases in culture volumes during cultivation were recorded via the BR1000 data logging system. Sampling was generally collected every 12 h for CHL-YN cells and every 24 h for CHO-K1 cell cultures. Additional samples were collected to monitor glucose levels during the metabolic shift. Viable cell concentration and cell viability were determined using a Vi-CELL[™] XR cell viability analyzer (Beckman Coulter). Extracellular metabolites, including glucose, lactate, glutamine, glutamate, and ammonia, were measured using a YSI2950 biochemistry analyzer (Xylem Inc.). IgG1 concentrations were measured using sandwich enzyme-linked immunosorbent assay techniques with a goat anti-human IgG Fc fragment (Bethyl Laboratories) as a primary antibody and a horseradish peroxidase-conjugated goat anti-human IgG Fc fragment (Bethyl Laboratories) as a secondary antibody. Finally, specific growth, production, and extracellular metabolite rates were calculated as previously described (Omasa et al., 1992).

2.3 | Automated and dynamic glucose feed control

Glucose concentration in the BR1000 bioreactor scale CHL-YN-IgG1 and CHO-K1-IgG1 cell cultivations was controlled at the setpoint of 3.0 ± 1.0 g/L using automated and dynamic glucose feeding strategies. The automated glucose feed used here is a predictive, closed-loop model control that was previously described by Sakaki et al. (2023). The glucose control system design includes a reference model established from preliminary culture data and a tuner algorithm, which enables determination of glucose feed rates following the

collection of in-line glucose and viable cell concentration data measured by near-infrared (NIR) spectroscopy and a capacitance sensor, respectively. The dynamic glucose feed strategy involves manual continuous glucose feeding calculated from offline glucose concentrations. The glucose feed volume was estimated from preliminary fed-batch culture data on each cell line. To evaluate the glucose feed volume (V_F), the amount of consumed glucose was first calculated via Equation (1). The V_F values were then calculated from Equation (2), from which the final glucose concentration (G_t) was set at 3.0 g/L. Finally, a graph of the time course of cumulative glucose feed volume was plotted to evaluate the glucose feed rate by linear regression.

$$\Sigma G = V_{t-1}G_{t-1} - V_tG_t + FV_F. \quad (1)$$

Equation (1) shows how to calculate the amount (g) of glucose consumed by cells (ΣG), where V is the cell culture volume (L), G is the glucose concentration of the cell culture (g/L), F is the glucose concentration of the glucose feed solution at 300.0 g/L, V_F is the glucose feed volume (L), and t is the time point (h).

$$G_t = \frac{V_{t-1}G_{t-1} - \Sigma G + FV_F}{V_{t-1} + V_F + V_{\text{others}}}. \quad (2)$$

Equation (2) shows how to calculate the V_F that should be added to achieve the 3.0 g/L G_t at a time point t , where V_{t-1} is the cell culture volume at $t-1$, G_{t-1} is the glucose concentration in the cell culture at $t-1$, ΣG is the amount of consumed glucose in grams (g) calculated from Equation (1), and V_{others} is the volume of other feeds added into the cell culture, which included feed medium (EX-CELL[®] Advanced CHO Feed 1) not containing glucose, and alkali solution.

Glucose feed rate modification was applied to compensate for the different glucose feed amounts resulting from cell culture variability and to improve the accuracy of the dynamic glucose feed control.

This modification was calculated using Equation (3), where the modified glucose feed $F_{\text{Gluc mod}}$ (L) comprises the set glucose feed amount $F_{\text{Gluc set}}$ (L) evaluated from the dynamic glucose feed design, the difference between the offline measurement and the setpoint of glucose concentration ΔG (g/L), the culture volume V (L), and the offline glucose concentration G (g/L).

$$F_{\text{Gluc mod}} = F_{\text{Gluc set}} + \left(\frac{\Delta G \cdot V}{G} \right). \quad (3)$$

Automated glucose feed operation was started on Day 1 of cultivation. Dynamic glucose feed control was started when the extracellular glucose concentration in cell cultures fell below 4.5 g/L.

2.4 | Sample pretreatment for metabolomics analyses

We analyzed samples from each cell culture at four different time points. As a CHL-YN-IgG1 cell model, CHL-YN-IgG1 cell pool and

CHL-YN B-08 samples were collected on Days 2–5. CHO-K1-IgG1 cell pool samples were collected on Days 2, 4, 6, and 8, to represent the early, exponential, stationary, and declining phases of cell growth, respectively. The supernatant and live cells of each sample were separated for extracellular and intracellular metabolomics analyses, respectively.

For the extracellular metabolomics analysis, cell culture supernatants were pretreated with acetonitrile (FUJIFILM Wako Pure Chemical) to precipitate proteins, followed by centrifugation at 15,000 rpm for 15 min at room temperature. The supernatants were collected and diluted 10-fold with ultrapure water. Finally, samples were analyzed using liquid chromatography (LC) with tandem mass spectrometry (LC-MS/MS) on an LCMS-8060NX triple quadrupole mass spectrometer, employing the LC/MS/MS Method Package for Cell Culture Profiling Ver. 3 (Shimadzu Corp.).

Cell samples for intracellular metabolomics analysis containing 1×10^7 living cells were washed with 5% D(-)-mannitol solution (FUJIFILM Wako Pure Chemical), then extracted with 99.7% methanol of LC-mass spectrometry (LC-MS) grade (FUJIFILM Wako Pure Chemical) before adding internal standard solution from Human Metabolome Technologies, Inc. The extracted cell solution was centrifuged at 2300g for 5 min at 4°C. The supernatant was transferred to a centrifugal filter column unit (Human Metabolome Technologies, Inc.) and centrifuged at 9100g for 180 min at 4°C. Filtrate samples were stored at -80°C and used to analyze intracellular metabolites by the capillary-electrophoresis and mass spectrometry (CE-MS) method via CE-time of flight (TOF)MS and CE-triple quadrupole mass spectrometry (QqQMS) analyses.

2.5 | Data processing, statistical analysis, and enrichment analysis

The extracellular metabolite data set was obtained from peak identification of the measured LC-MS data via LabSolutions Insight™ LCMS data analysis software with the Peakintelligence™ algorithm, which incorporates assistance from artificial intelligence to search for chromatography peaks (Shimadzu Corp.). Quantified extracellular metabolic data are displayed in terms of chromatographic peak area. While the raw data set of measured intracellular metabolites was provided by Human Metabolome Technologies, Inc. in units of pmol/10⁶ cells, Sample data were divided into three data sets by cultivation batches: (1) CHL-YN-IgG1 cell pool days 2, 3, 4, and 5; (2) CHL-YN B-08 clone days 2, 3, 4, and 5; and (3) CHO-K1-IgG1 cell pool days 2, 4, 6, and 8. Then, extracellular and intracellular metabolomics data were separately processed by R computational programming on the MetaboAnalyst 5.0 platform (www.metaboanalyst.ca). The datasets were processed by removing features with >75% missing values followed by auto-scaling, which was mean-centered and divided by the standard deviation of each variable. After that, statistical analyses were also conducted on the MetaboAnalyst 5.0 platform.

To visualize data overview, principal component analysis (PCA) was used to examine differences between samples. All samples were

subjected to PCA and generally categorized by K-means clustering and hierarchical clustering analysis (HCA), which used an average clustering algorithm and Spearman's rank correlation coefficient as the distance measurement. Detailed analyses were then conducted to collect more information, after which the PCAs were re-processed to observe distinctions between CHL-YN-IgG1 and CHO-K1-IgG1 cell pools during the glutamine production phase, and within the CHL-YN cell models (CHL-YN-IgG1 cell pool and CHL-YN B-08) during the glutamine consumption and production phases. Samples were clustered by K-means analysis. Fold change (FC) and statistical significance (*p* value) analyses were then applied to highlight the significantly different metabolites between sample groups on a volcano plot.

Different metabolites were further subjected to over-representation analysis (Vodopivec et al., 2019) to evaluate the probability of involvement of related metabolic pathways in the selected pathway database. The list of upregulated and down-regulated metabolites from the volcano plot was evaluated through the reduced version of the Chinese hamster (*C. griseus*) metabolic pathways map in the Kyoto Encyclopedia of Genes and Genomes (KEGG) database. The selected CHO cell database was searched to identify measured target metabolites that were over-represented.

3 | RESULTS

3.1 | Glucose feed strategies evaluation for fed-batch IgG1-producing CHL-YN cell cultures

An IgG1-producing CHL-YN cell pool was selected as a model to study glucose feed control strategies in serum-free fed-batch operation. The NIR spectroscopy-based glucose monitoring and automated glucose feed control system was initially established on the basis of a preliminary culture experiment (data not shown). Using automated glucose feed control, CHL-YN cells could be cultivated for up to 9.5 days with over 70% viability. After reaching the maximum viable cell concentration on Day 4, the viability of CHL-YN cells started to decrease (Figure 1a). The extracellular glucose measurements revealed that glucose was rapidly consumed from Day 2 onward, dropping precipitously between Days 2 and 3. On Day 3.5, glucose demand suddenly dropped, resulting in glucose overfeeding in the automated glucose feed cultures (Figure 1b). The reduction in consumed glucose may have been supported by the lactate switch from production to consumption, which occurred at Day 3.5 as well (Figure 1c). Glucose overfeeding indicated that a metabolic change in the CHL-YN cells might have occurred on Day 3.5. Coincident with the shift in glucose consumption, extracellular glutamine became depleted and subsequently increased on Day 3.5 (Figure 1d). Therefore, we hypothesized that the metabolic switch in glutamine from consumption to production might have been related to the change in glucose consumption. Development of the dynamic glucose feed control system for CHL-YN cells was then aimed at stabilizing the glucose concentration.

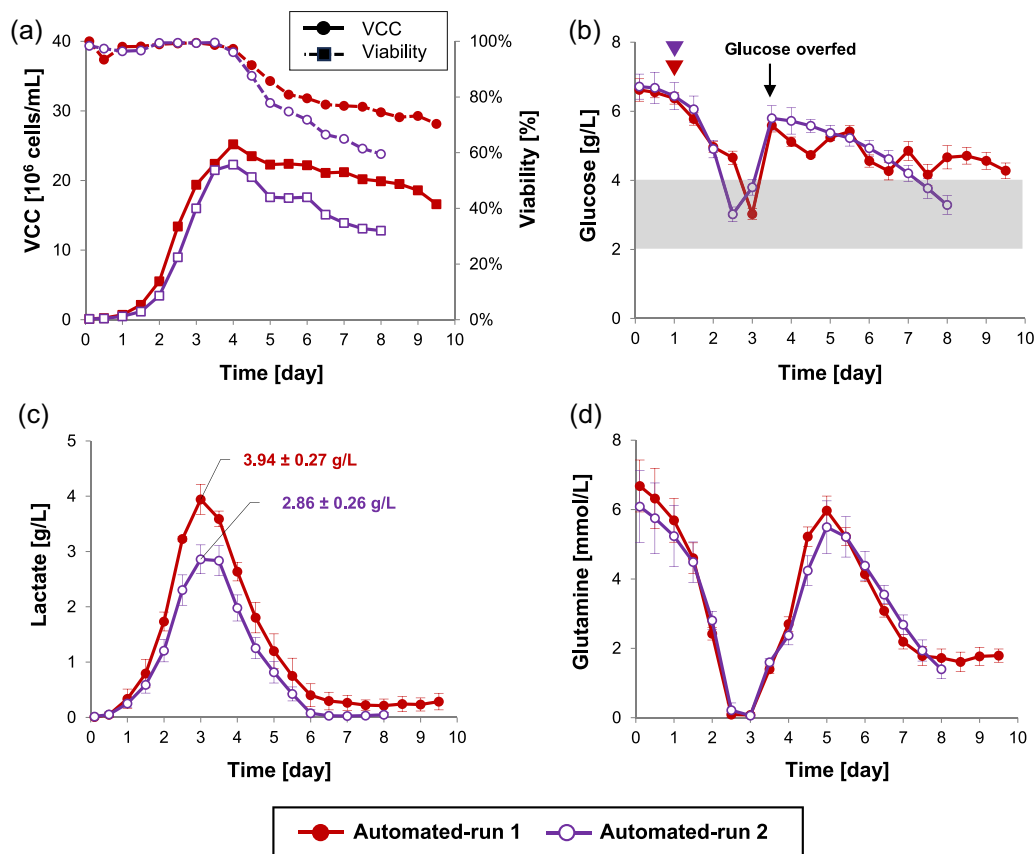


FIGURE 1 Cell culture profiles of automated glucose feed control of fed-batch Chinese hamster lung (CHL)-YN-immunoglobulin G (Ig)G1 cell cultures. (a) Time course of viable cell concentration (VCC; solid line) and cell viability (dashed line). (b) Time course of extracellular glucose measurement. The gray area represents the range of dynamic glucose feeding that was found to control glucose (3.0 ± 1.0 g/L). An arrow indicates the glucose overfeeding available on Day 3.5. Arrowheads indicate the starting point of the glucose feed operation. (c) Time course of extracellular lactate measurement. Data labels indicate the peak lactate concentration on Day 3 of duplicate runs. (d) Time course of extracellular glutamine measurement, illustrating the glutamine switch from consumption to production that occurred mainly on Day 3. Bioreactor cultivations were performed in duplicate runs. Extracellular metabolite concentrations are displayed with error bars representing the standard deviations from triplicate measurement ($n = 3$).

3.2 | Development of dynamic glucose feed control

The dynamic glucose feed design for CHL-YN cells was achieved by evaluating the glucose feed rates from a plot of the time course of cumulative glucose feed volume. The CHL-YN-IgG1 cell pool cultures were divided into three phases with the following optimized dynamic glucose feed rates: 31.9, 8.62, and 18.0 mL/d on Days 2–4, Days 4–6, and postday 6, respectively (Figure 2a). The dynamic glucose feed control was also applied to the CHL-YN B-08 clone and CHO-K1-IgG1 cell pool cultures. The CHL-YN B-08 cultures were divided into three distinct phases with the following dynamic glucose feed rates: 24.3, 7.15, and 18.4 mL/day on Days 2–4, Days 4–6, and postday 6, respectively (Figure 2b). By contrast, the calculated glucose feed rate of the CHO-K1 cell cultures remained at a constant rate of 21.5 mL/day from Day 2 of the cultivation onwards (Figure 2c). These results suggest that the glucose consumption patterns of CHL-YN cells were distinctly different from those of CHO-K1 cells. Under dynamic glucose feed control, both the IgG1 cell pool and B-08 clone of

CHL-YN were able to be controlled within a range of 3.00 ± 1.00 g/L glucose.

3.3 | Cultivation profiling of IgG1-producing CHL-YN and CHO-K1 cell cultures with dynamic glucose feed control

Considering the dynamic glucose feed control fed-batch cultures, both the cell pool and B-08 clone of CHL-YN-IgG1 cells showed similar growth and metabolic profiles. Under a stabilized glucose condition, the CHL-YN cell lines were cultivated for up to 13 days with over 70% viability. In general, the viable cell concentration of the CHL-YN cells, including both the IgG1 cell pool and B-08 clone, reached a peak at about Day 4.5 of cultivation, while the CHO-K1 cell line reached a peak on Day 6 (Figure 3a). However, CHL-YN cell viability started to drop on Day 4, decreased considerably until Day 6, and then gradually decreased until the end of cultivation (Figure 3b). Regarding extracellular metabolite concentrations, glutamine in

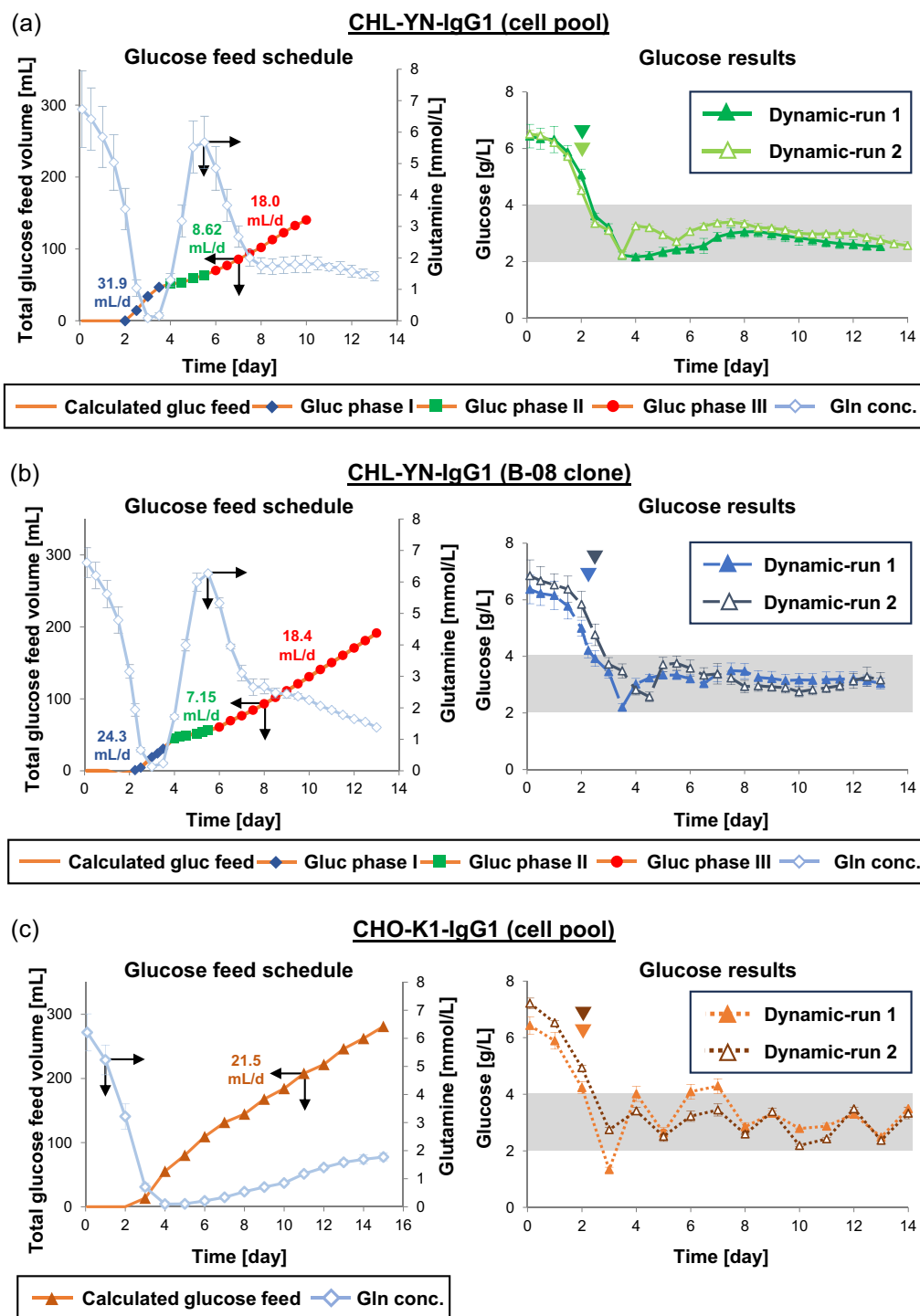


FIGURE 2 Design of dynamic glucose feed control strategies for the cell pool and B-08 clone of Chinese hamster lung (CHL)-YN-immunoglobulin G (Ig)G1 cells and the Chinese hamster ovary (CHO)-K1-IgG1 cell pool. (a-c) Dynamic glucose feed control strategies developed for the CHL-YN-IgG1 cell pool (a), the CHL-YN-IgG1 B-08 cell clone (b), and the CHO-K1-IgG1 cell pool (c). Graphs on the left illustrate the schedule of glucose feed rate estimated by linear regression from a time course of accumulated glucose feed volume, which showed an oscillation following glutamine metabolism only in CHL-YN cells. Graphs on the right illustrate the time course of extracellular glucose measurements during dynamic glucose feed control. Gray areas represent the range of dynamic glucose feeding that were found to control glucose (3.0 ± 1.0 g/L). Data on extracellular glucose and glutamine concentrations are displayed with error bars representing the standard deviations from triplicate measurement ($n = 3$). Arrowheads indicate the starting point of the glucose feed operation. Bioreactor cultivations were performed in duplicate runs.

CHL-YN cultures of both the cell pool and B-08 clone was consumed for 3 days before becoming depleted; it was then produced from Days 3–5.5, then began to be re-consumed and remained stable until the end of the cultivation. By contrast, in CHO-K1 cell cultures, glutamine was only slightly increased after being depleted on Day 4 (Figure 4a). Lactate was produced at a lower level by the CHL-YN cell line than by the CHO-K1 cell line. Furthermore, there was also a shift in lactate from production to consumption that occurred on Day 3.5 in CHL-YN (12 h after glutamine depletion), and on Day 5 in CHO-K1 (24 h after glutamine depletion). However, lactate depletion was only observed in CHL-YN cell cultures (Figure 4b).

Additionally, glutamate and ammonia shifted concordantly, similar to the glutamine profile, in CHL-YN. In CHL-YN cell cultures, glutamate dropped, and ammonia decreased on Day 3; as glutamate approached depletion, ammonia started increasing again (Figure 4c,d). IgG1 production during two dynamic runs varied across the cultures: the CHL-YN B-08 clone produced the highest IgG1 concentrations, at 146 and 134 mg/L; the CHL-YN IgG1 cell pool produced 67.9 and 62.0 mg/L; and the CHO-K1 cell pool produced only 18.4 and 16.8 mg/L IgG1 (Figure 4e). These results uncovered greater challenges in IgG production in the CHL-YN cell line than in the CHO-K1 cell line; namely, earlier decrease in viability and fluctuation in ammonia production, which was highly released during late cultivation of CHL-YN cells. In addition, run 2 of the CHL-YN

B-08 clone had a longer lag phase, leading to delays in cell growth and metabolism. The cause of the longer lag phase was unclear.

Specific evaluations of the glucose and glutamine consumption rates indicated that the oscillation in glucose consumption in CHL-YN cells followed changes in glutamine metabolism within a 12-h timeframe. There was evidence of a glutamine-dependent glucose consumption shift in CHO-K1 cells as well; however, it showed a different pattern.

To evaluate the specific glucose consumption rates, the ideal glucose amount, excluding the influences of glucose feed ($VG_{\text{gluc}} - f_{\text{FG}_F} dt$) and integral viable cell concentration ($\int VX, dt$), was plotted. Distinct glucose consumption rates were apparent at the four growth phases (I–IV) of the CHL-YN cell pool and B-08 clone, but were only apparent at phases I and II of the CHO-K1 cell pool. Glucose consumption of CHL-YN cell cultures was high at the beginning of cultivation (phase I), dropped thereafter, and stayed low on Days 3.5–6 (phase II), increased on Days 6–9 (phase III), and slightly increased further from Day 9 until the end of cultivation (phase IV). By contrast, glucose consumption in CHO-K1 cell cultures was high at the beginning of cultivation (phase I), then dropped from Day 4 until the end of cultivation (phase II) (Table 1 [A]). These findings suggest that CHO-K1 consumed glucose at higher levels than CHL-YN cells in phase I. In addition, the very low glucose consumption pattern in phase II of CHL-YN cell cultures was not observed in CHO-K1 cell cultures.

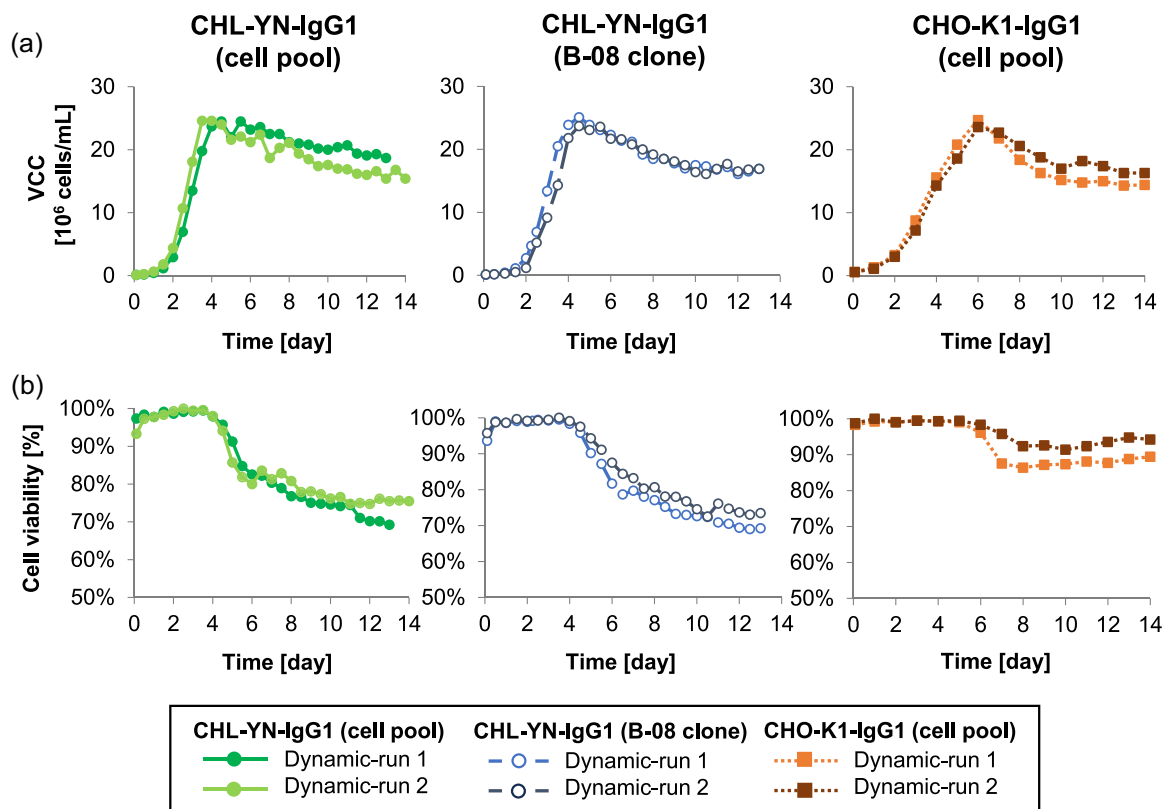


FIGURE 3 Cell culture profiles of dynamic glucose feed control of fed-batch cultivations of the cell pool and B-08 clone of Chinese hamster lung (CHL)-YN-immunoglobulin G (Ig)G1 cells and the Chinese hamster ovary (CHO)-K1-IgG1 cell pool. (a) Time course of viable cell concentration (VCC). (b) Cell viability. Bioreactor cultivations were performed in duplicate runs.

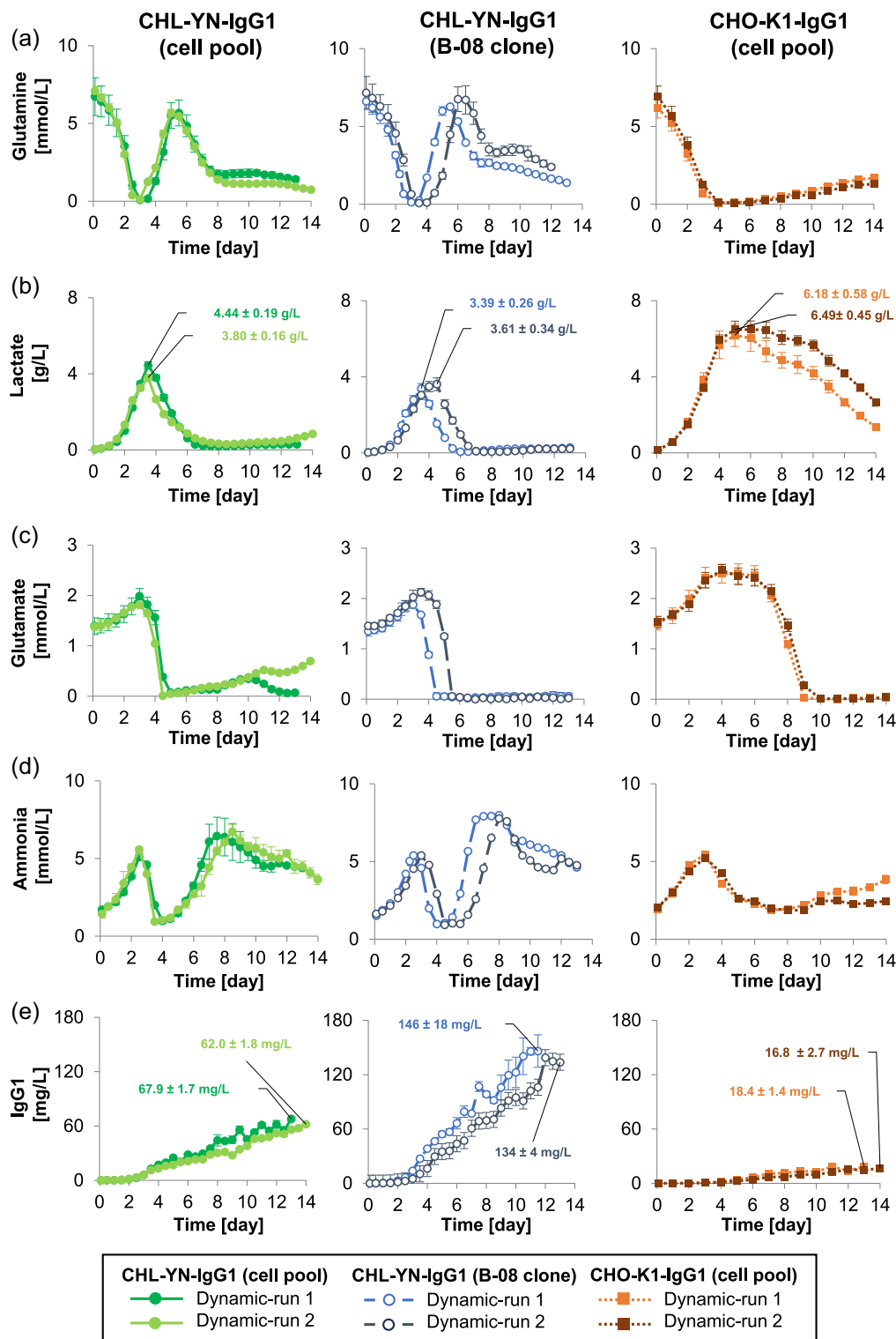


FIGURE 4 Concentrations of extracellular metabolites during dynamic glucose feed control of fed-batch cultures of the cell pool and B-08 clone of Chinese hamster lung (CHL)-YN-immunoglobulin G (Ig)G1 cells and the Chinese hamster ovary (CHO)-K1-IgG1 cell pool. (a–e) Time course of measurement of extracellular metabolites: glutamine (a), lactate (b), glutamate (c), ammonia (d), and IgG1 (e). Data labels in (b) and (e) indicate the peak in lactate concentration and final IgG concentration, respectively. Data expressed as concentration \pm standard deviation. Bioreactor cultivations were performed in duplicate runs. Extracellular metabolites and IgG1 were measured in triplicate ($n = 3$).

TABLE 1 Specific rate calculation of fed-batch cell pool and B-08 clone of Chinese hamster lung (CHL)-YN-immunoglobulin G (Ig)G1 cells and the Chinese hamster ovary (CHO)-K1-IgG1 cell pool cultivations.

(A) Specific glucose consumption rates [pmol cell ⁻¹ day ⁻¹]				
	Phase I (1–3.5 days)	Phase II (3.5–6 days)	Phase III (6–9 days)	Phase IV (9 days–end)
Dynamic glucose feed control				
CHL-YN-IgG1 cells				
Cell pool–run 1	3.21 ± 0.14	0.24 ± 0.01	0.50 ± 0.01	0.63 ± 0.01
Cell pool–run 2	3.29 ± 0.03	0.34 ± 0.02	0.53 ± 0.02	0.75 ± 0.01
B-08 clone–run 1	2.67 ± 0.15	0.26 ± 0.01	0.59 ± 0.02	0.77 ± 0.00
B-08 clone–run 2 ^a	3.47 ± 0.11	0.23 ± 0.01	0.62 ± 0.02	0.81 ± 0.02
	Phase I (1–4 days)	Phase II (4 days–end)		
Dynamic glucose feed control				
CHO-K1-IgG1 cells				
Cell pool–run 1	3.77 ± 0.12	0.67 ± 0.01		
Cell pool–run 2	4.20 ± 0.03	0.69 ± 0.01		
(B) Specific glutamine consumption rate [pmol cell ⁻¹ day ⁻¹]				
	Gln consumption (1–3 days)	Gln production (3.5–5.5 days)	Gln re-consumption (5.5–8 days)	Gln stable (8 days–end)
Dynamic glucose feed control				
CHL-YN-IgG1 cells				
Cell pool–run 1	1.18 ± 0.18	–0.16 ± 0.02	0.08 ± 0.01	0.001 ± 0.001
Cell pool–run 2	0.90 ± 0.04	–0.16 ± 0.02	0.08 ± 0.00	0.002 ± 0.000
B-08 clone–run 1	1.27 ± 0.10	–0.17 ± 0.01	0.08 ± 0.01	0.012 ± 0.001
B-08 clone–run 2 ^b	1.57 ± 0.21	–0.16 ± 0.02	0.10 ± 0.02	0.016 ± 0.001
	Gln consumption (1–4 days)	Gln production (4 days–end)		
Dynamic glucose feed control				
CHO-K1-IgG1 cells				
Cell pool–run 1	0.50 ± 0.05	–0.01 ± 0.00		
Cell pool–run 2	0.56 ± 0.07	–0.01 ± 0.00		
(C) Specific productivity [pg cell ⁻¹ day ⁻¹]				
	Gln consumption (1–3 days)		Gln production (3.5–5.5 days)	Gln re-consumption (5.5–8 days)
Automated glucose feed control				
CHL-YN-IgG1 cells				
Cell pool–run 1	0.42 ± 0.02		0.16 ± 0.02	0.27 ± 0.02
Cell pool–run 2	0.58 ± 0.01		0.19 ± 0.04	0.35 ± 0.03
Dynamic glucose feed control				
CHL-YN-IgG1 cells				
Cell pool–run 1	0.65 ± 0.02		0.26 ± 0.02	0.33 ± 0.08
Cell pool–run 2	0.44 ± 0.03		0.18 ± 0.01	0.20 ± 0.03
B-08 clone–run 1	1.51 ± 0.09		0.63 ± 0.04	0.89 ± 0.03
B-08 clone–run 2 ^b	1.41 ± 0.02		0.50 ± 0.03	0.56 ± 0.01

(Continues)

	Gln consumption (1–4 days)	Gln production (4 days–end)
Dynamic glucose feed control		
CHO-K1-IgG1 cells		
Cell pool–run 1	0.09 ± 0.01	0.08 ± 0.01
Cell pool–run 2	0.05 ± 0.01	0.08 ± 0.01

Note: (A) Specific glucose consumption rates. (B) Specific glutamine consumption rates. (C) Specific productivity.

^aRates calculated based on a graph pattern, which showed a 1-day delay in glucose consumption; phase I (1–4.5 days), phase II (4.5–7 days), phase III (7–10 days), and phase IV (10 days–end).

^bRates calculated based on a graph pattern, which showed a delay in glutamine consumption; glutamine consumption (1–3.5 days), glutamine production (4–6.5 days), glutamine re-consumption (6.5–8.5 days), cell decline (8.5 days–end).

Specific glutamine consumption rates were evaluated by linear regression of the plot of the glutamine amount (VG_{gln}) and $\int VX_v dt$. In CHL-YN cell cultures, the specific glutamine consumption rates illustrated the fluctuations in glutamine metabolism, which were divided into three active phases: consumption, production, and re-consumption. Glutamine consumption was at a high level on Days 1–3; extracellular glutamine showed depletion on Day 3; glutamine production occurred on Days 3.5–5.5, after which glutamine re-consumption began; and, from Day 8 onward, glutamine consumption was reduced, but remained stable at a very low level. In contrast, specific glutamine consumption of CHO-K1 cell cultures was apparent at only two phases: high glutamine consumption during early cultivation (Days 1–4) until glutamine depletion on Day 4; and glutamine production from Day 4 to the end of cultivation (Table 1 [B]). These findings demonstrated that CHL-YN cells consumed glutamine at higher levels than did CHO-K1 cells in the early stage. After that, CHL-YN cells produced over 10-fold more glutamine than CHO-K1 cells following glutamine depletion. Only CHL-YN cell cultures displayed a glutamine re-consumption stage. Additionally, specific productivity evaluation suggested that IgG1 production of CHL-YN cells also fluctuated following glutamine metabolism, as well as the glucose consumption pattern. CHL-YN cells had the highest productivity during the glutamine consumption phase. After that, the productivity was reduced during glutamine production and slightly increased during the glutamine re-consumption phase (Table 1 [C]).

Compared with previous CHL-YN-IgG1 cell pool cultures grown in batch and bolus fed-batch and using several methodologies, the dynamic glucose feed control system prolonged the cultivation to up to 13 days with over 70% cell viability and improved the final quantitative IgG1 production from 6.47 mg/L in batch and 23.0 mg/L in bolus fed-batch to up to 66.7 mg/L (Supporting Information S2: Table 1). Furthermore, the first successfully cultivated single-clone isolate of CHL-YN cells exhibited improved IgG1 production (up to 146 mg/L) and confirmed the feasibility of generating a high-production clone. However, in terms of specific productivity, the results suggest that IgG1 productivity of CHL-YN cells could not be increased by using dynamic glucose feed control.

3.4 | Targeted extracellular metabolomics analysis

Since the reduction in CHL-YN viability occurred during the first glutamine metabolic shift from consumption to production, targeted metabolomics analysis of central carbon-associated metabolites and intermediates was performed to explore extracellular components that may have a critical impact on CHL-YN cell cultures during this transition state. Supernatant collected from dynamic glucose fed-batch cultures of the CHL-YN-IgG1 cell pool, CHL-YN B-08 clone, and CHO-K1-IgG1 cell pool covering the first-glutamine metabolic shift were used for LC-MS/MS analysis (Figure 5a). LC-MS/MS quantitative measurements detected 136 of a total of 144 targeted compounds. After that, the 136 raw metabolomics data were processed by auto-scaling before conducting statistical analyses (Supporting Information: S1). PCA provided an overview of extracellular metabolic profiles detected in each sample (Figure 5b). Additionally, the data were clustered by K-means analysis and HCA (Figure 5c), both of which highlighted three distinct groups: CHL-YN and CHO-K1 cell lines before glutamine depletion (CHL-YN IgG1 cell pool and B-08 on Days 2 and 3; and CHO-K1 cell pool on Days 2 and 4); CHL-YN cell line after glutamine depletion (CHL-YN IgG1 cell pool and B-08 on Days 4 and 5); and CHO-K1 cell line after glutamine depletion (CHO-K1 cell pool on Days 6 and 8). These results suggest that CHL-YN cells and CHO-K1 cells exhibited different metabolic profiles following glutamine depletion.

3.5 | Comparison of extracellular metabolites between CHL-YN and CHO-K1 during glutamine production

To further examine the different glutamine production profiles in CHL-YN and CHO-K1 cells, we searched for differentially produced compounds from a volcano plot illustrating metabolites with significant between-sample differences using cutoffs of $\log_2\text{-FC}$ ($\text{FC} > 2.0$) and $-\log_{10} p$ value ($p < 0.05$) (Supporting Information S2: Figure 1). There were 24 metabolites detected at higher levels and 39 metabolites detected at lower levels in

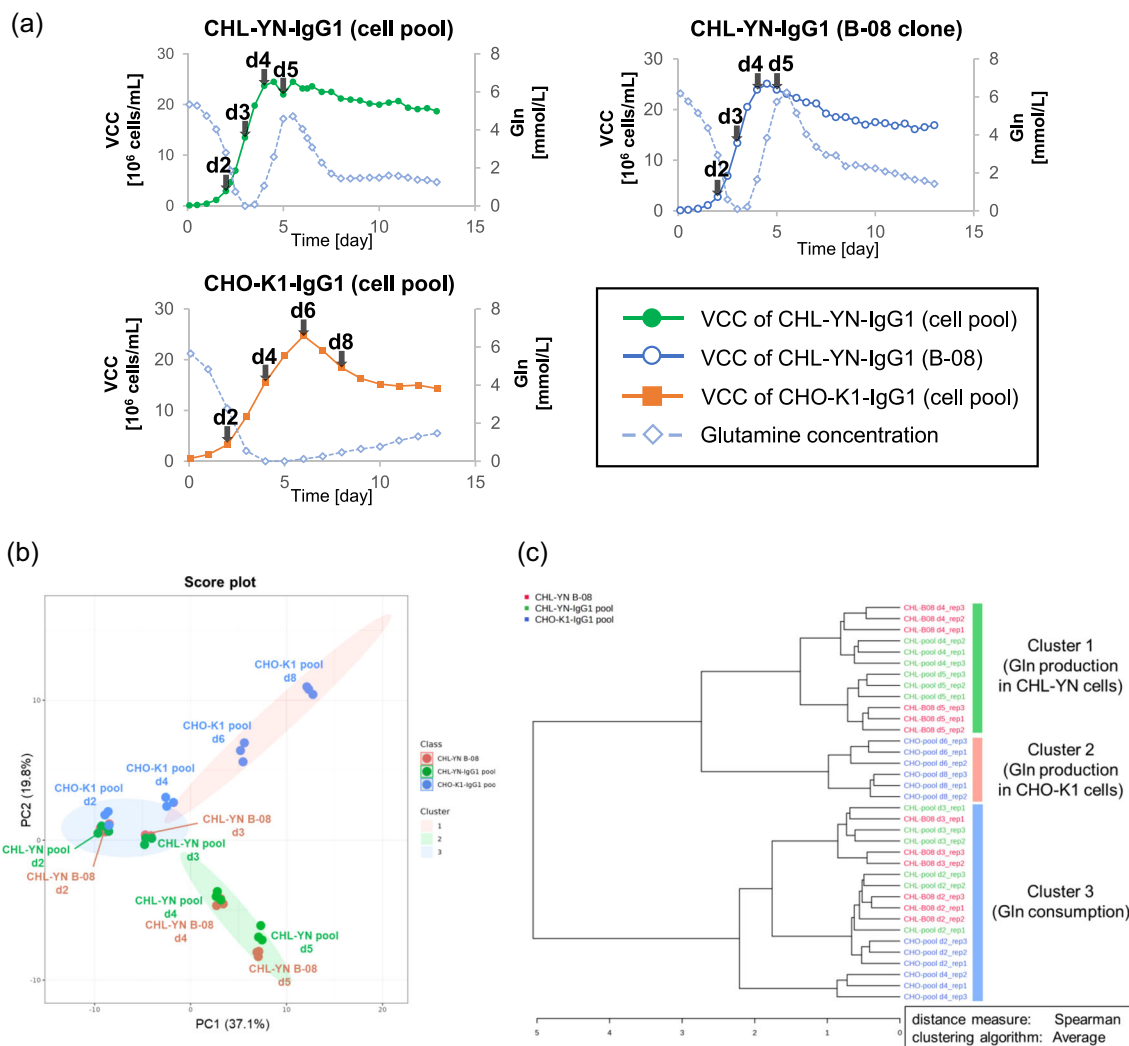


FIGURE 5 Overview of liquid chromatography with tandem mass spectrometry-based targeted extracellular metabolomics analysis. (a) Viable cell concentrations (VCC) of the cell pool and B-08 clone of Chinese hamster lung (CHL)-YN-immunoglobulin G (IgG1) cells and Chinese hamster ovary (CHO)-K1-IgG cell pool samples collected for extracellular metabolomics analysis of the early exponential, late exponential, stationary, and decline phases of growth. Supernatant samples of CHL-YN cells were collected at 48 h (Day 2 [d2]), 72 h (d3), 96 h (d4), and 120 h (d5), while those of CHO-K1 cells were collected at 48 h (d2), 96 h (d4), 144 h (d6), and 192 h (d8). (b) Principal component analysis (PCA) plot illustrating the measurement of 136 metabolites in a single compact dot. Clusters were determined from K-means clustering analysis. (c) Hierarchical clustering analysis (HCA) plot showing the distinct metabolic information in each sample. An average clustering algorithm and Spearman's rank correlation coefficient method were selected for the HCA. Gln, glutamine.

CHL-YN cell cultures compared with those in CHO-K1 cell cultures. Among the significant metabolites, several were involved in arginine metabolism (urea cycle, proline metabolism, and polyamine biosynthesis) and cysteine and methionine metabolism. The five amino acids showing the highest FC values were glutamine, methionine, arginine, aspartate, and proline (Table 2 [A]). In addition, the top 10 overall metabolites included four arginine metabolic compounds (ornithine, citrulline, putrescine, and argininosuccinate) and two cysteine and methionine metabolites (cystathionine and glutathione) (Table 2 [B]). These results suggest that CHL-YN and CHO-K1 cells may exhibit strong differences in these metabolic backgrounds.

3.6 | Hypothesized models created from deprived amino acids and associated metabolic profiling of CHL-YN cells during glutamine production

Our initial examination of metabolic characteristics was focused on amino acids. The intracellular metabolomics analysis was similar to the extracellular metabolomics analysis (Supporting Information: S1 and Supporting information S2: Figure 2) and produced concordant results. Analysis of the combined metabolomics results showed that the concentrations of nine amino acids (arginine, aspartate, isoleucine, leucine, methionine, phenylalanine, serine, tyrosine, and valine) in both the cell pool and B-08 clone of CHL-YN cell cultures decreased during the

TABLE 2 Extracellular metabolites with the highest significant fold differences between Chinese hamster lung (CHL)-YN cells and Chinese hamster ovary (CHO)-K1 cells following glutamine depletion.

(A) Amino acids
Glutamine
Methionine
Arginine
Aspartate
Proline
(B) Metabolic components
Deoxycytidine
Cystathionine
Uridine
Homocysteine
Glutathione (GSH)
Ornithine
Cytidine
Citrulline
Putrescine
Argininosuccinate

Note: (A) Top five extracellular amino acids. (B) Top 10 extracellular metabolites.

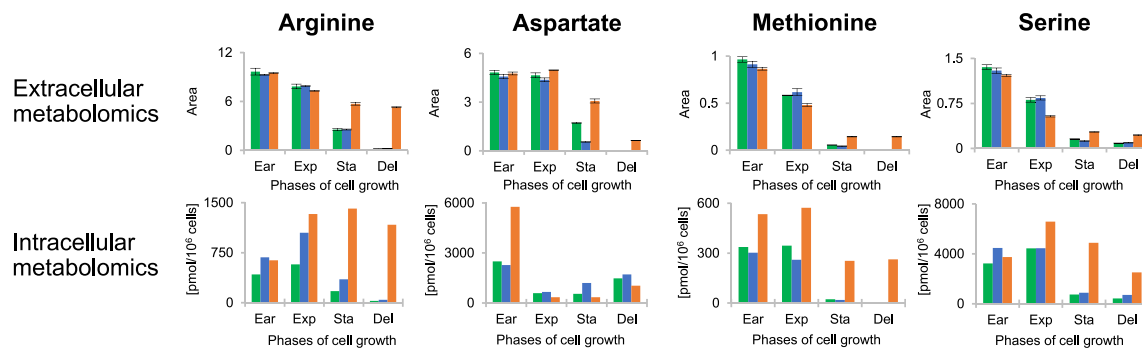
glutamine metabolic shift between Days 3 and 4 (Supporting information S2: Figures 3 and 4). Additionally, the concentrations of four of these amino acids (arginine, aspartate, methionine, and serine) dropped sharply on Day 4, and then decreased to near depletion on Day 5 (Figure 6a). These results suggest that these four amino acids were highly utilized in CHL-YN cells during the glutamine shift. High amino acid catabolic activities and deprivation of these amino acids may be critically related to the reduction in CHL-YN cell viability. This metabolomics study also revealed that CHL-YN cells had higher demands for arginine and methionine than CHO-K1 cells.

The concentrations of arginine metabolic derivatives revealed the unique characteristics of CHL-YN cells. Ornithine and citrulline, intermediates of the urea cycle, increased with each phase of cell growth, whereas argininosuccinate steadily declined with each phase in CHL-YN cells. High production of ornithine in CHL-YN cells seemed to correlate with several associated pathway components, including proline, glutamate, glutamine, polyamines (putrescine), and 4-aminobutyrate (GABA) (Figure 6b). These results may suggest that high glutamine production in CHL-YN cells is related to high ornithine production. Intriguingly, intracellular proline concentrations increased in parallel with increases in extracellular proline during cultivation, suggesting that CHL-YN cells may possess proline biosynthesis ability.

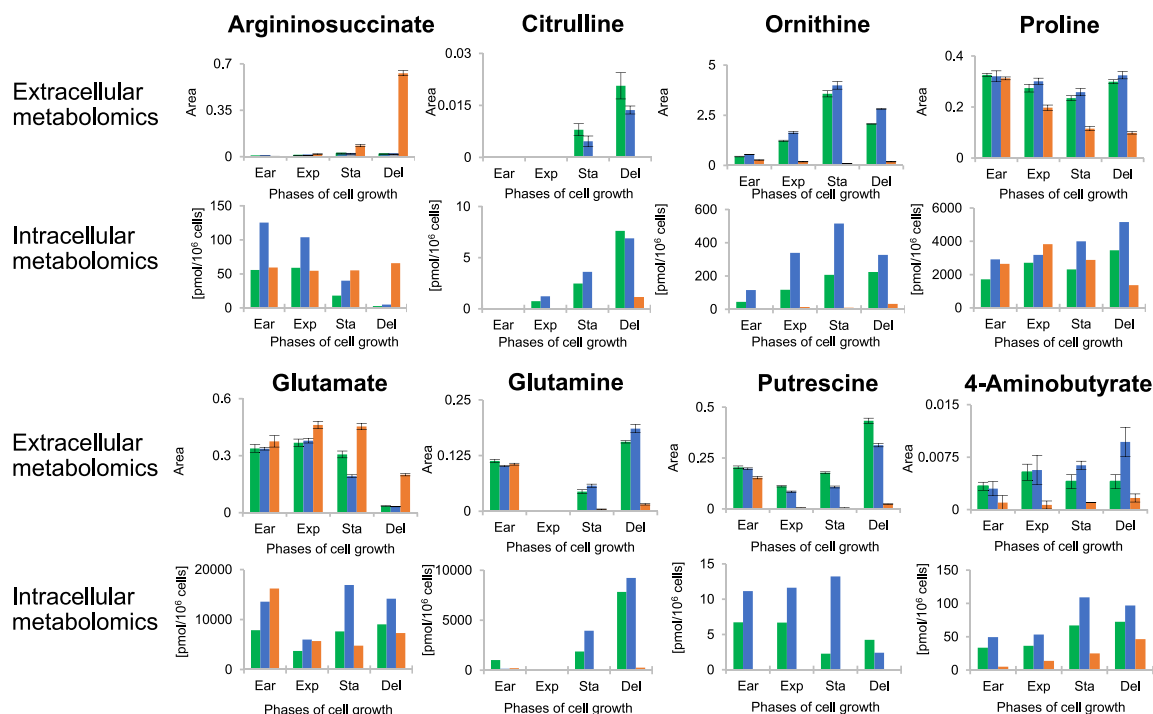
Cysteine production ability was also observed in CHL-YN cells. High concentrations of cystathionine, a precursor of cysteine biosynthesis, were found in both intracellular and extracellular samples of CHL-YN cells, but not those of CHO-K1 cells. This finding correlated with the high methionine and serine requirements of CHL-YN cells. However, the cysteine concentration could not be reliably reported because of rapid oxidation. Cysteine production leads to increased concentrations of intracellular glutathione (GSH), an important tripeptide antioxidant. The ratio of GSH to oxidized GSH (GSSG) was also higher in CHL-YN cells than in CHO-K1 cells (Figure 6c).

In addition to the above, our group previously reported (Yamano-Adachi et al., 2020) the mRNA expression of genes in host CHL-YN and CHO-K1 cells cultivated in serum-free flask-batch operation using the same flask-scale cultivation procedure described in this study, that is EX-CELL[®] CD CHO Fusion medium (Merck) containing 6 mM L-glutamine. The results of that RNA sequence analysis support our hypotheses about the distinct differences in arginine and methionine metabolism in CHL-YN cells. Normalization of those mRNA expressions revealed that several associated enzymes were more highly expressed in CHL-YN cells than in CHO-K1 cells (Supporting Information S2: Table 2). For instance, arginase-2 (ARG-2) and cystathionine γ -lyase (CTH) displayed high expression in CHL-YN cells and no detectable expression in CHO-K1 cells. Furthermore, during the exponential phase, argininosuccinate synthetase, ornithine decarboxylase, aldehyde dehydrogenase 18 family member A1 (P5CS), and cystathionine β -synthetase (CBS) were expressed at levels fivefold higher in CHL-YN cells than in CHO-K1 cells. Hence, we established hypothesized models of arginine (Figure 7) and methionine (Figure 8) metabolism in the two cell lines. CHL-YN cells possessed the ability to convert arginine to ornithine via ARG-2, affecting the generation of several urea cycle products and related derivatives, including glutamine, proline, and putrescine. Furthermore, based on their expression of methionine adenosyltransferase 2A (MAT2A), methyltransferases, adenosyl homocysteinase, CBS, and CTH, CHL-YN cells might be able to completely biosynthesize cysteine. Higher cysteine biosynthesis ability could lead to enhanced GSH production. CHO-K1 cells, which did not express ARG-2, lacked the ability to convert arginine to ornithine and thus did not produce detectable levels of derivatives such as citrulline and putrescine. Although we observed expression of genes related to glutamate 5-semialdehyde in CHO-K1 cells, extracellular and intracellular metabolomics analysis suggest a pattern of proline uptake only, indicating that these cells might not produce proline. Additionally, CHO-K1 cells showed very low CBS gene expression and lacked CTH gene expression, suggesting that cysteine production was disabled. The metabolic results were confirmed by LC-MS/MS-based extracellular and intracellular metabolomics analysis of flask-batch CHL-YN-IgG1 and CHO-K1-IgG1 cell pools cultivated in EX-CELL[®] CD CHO Fusion supplemented 6 mM L-glutamine and 5 μ g/mL puromycin. These analyses showed similar patterns of arginine and methionine metabolic compounds in the dynamic glucose feed fed-batch experiment (Supporting information S2: Figures 5 and 6).

(a) **Deprived amino acids**



(b) **Arginine metabolism** (urea cycle, glutamate, proline, and polyamine biosynthesis)



(c) **Methionine metabolism** (methionine cycle and cysteine biosynthesis)

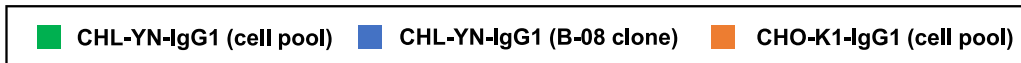
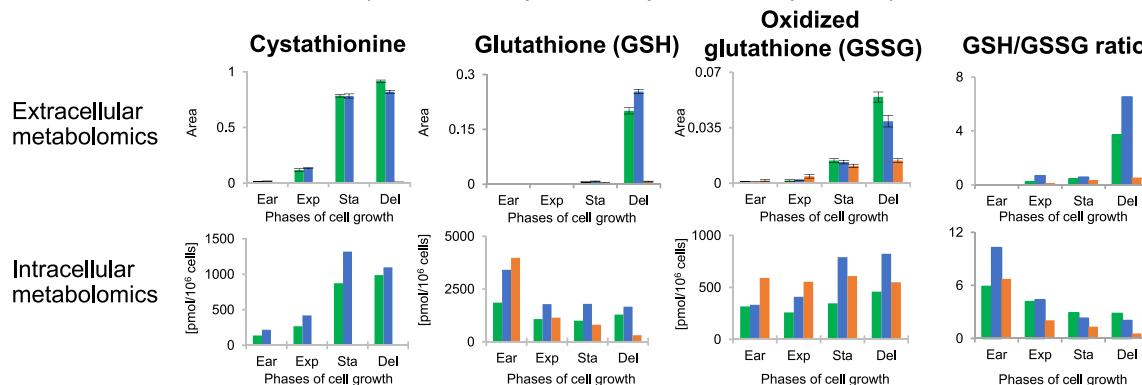


FIGURE 6 (See caption on next page).

4 | DISCUSSION

In this study, we introduced bioreactor-scale fed-batch cultivation of IgG1-producing CHL-YN cells and searched for glucose feed strategies that could provide stable glucose conditions. Initially, we selected automated glucose feed control for the CHL-YN cell cultures but found that glucose overfeeding occurred. We concluded that it is difficult to predict glucose concentrations in CHL-YN cell cultures using the current glucose consumption model because of their rapid glucose consumption during the growth phase and immediate drop in consumption after glutamine depletion. Currently, development of a new glucose consumption model for CHL-YN cells is in progress.

Next, we attempted to design a dynamic glucose feed strategy for CHL-YN cells based on specific glucose consumption rates, which oscillated following glutamine metabolism. As a result, we successfully controlled extracellular glucose at the target range (3 ± 1 g/L). This glucose range was based on the bolus fed-batch CHO cell culture, which supplied glucose up to a 4 g/L final concentration in the cell culture whenever the glucose concentration dropped below 2 g/L. Additionally, we reasoned that setting the minimum glucose concentration threshold at a lower point might risk glucose depletion because of the rapid consumption in the growth phase. This glucose control could prolong the cell viability over 70% up to 13 days, resulting in increased final IgG1 concentration. However, compared with automated glucose cultures, the maximum lactate concentrations in dynamic glucose feed control remained unchanged, suggesting that the 3 ± 1 g/L setting range did not present a low glucose condition. Therefore, the improved cell viability may have been due to prevention of a glucose overfeeding-mediated increase in osmotic pressure, which can affect both cell growth and productivity (Alhuthali et al., 2021).

The dynamic glucose feed control was also successfully designed for a high IgG1-producing clone, CHL-YN B-08. To date, dynamic glucose feed control of CHL-YN B-08 cell cultures can produce IgG1 concentrations of up to 146 mg/L, which is approximately 2.2-fold higher than CHL-YN cell pool with the same fed-batch culture conditions and 23-fold higher than the CHL-YN bioreactor-batch culture (6.47 mg/L). From a production perspective, CHL-YN is not yet competitive with current industrial cell lines, which produce IgG1 at final concentrations approaching g/L units. Thus, we conducted metabolomics analysis of extracellular cell culture components aimed at identifying critically limited metabolites, which could lead to a better understanding of the needs of CHL-YN cells and support further development of a feed strategy with improved culture

performance. In the future, the expression vector, promoter, and selection marker for large-scale production should also be optimized for CHL-YN cells.

The LC-MS/MS targeted extracellular metabolomics analysis was conducted to investigate CHL-YN cell culture components, focusing on the first glutamine shift. The overview of metabolites revealed that differences between CHL-YN and CHO-K1 cells began after extracellular glutamine depletion. The volcano plot indicated significant differences in several arginine and methionine metabolism-associated compounds. Metabolic profiles, including extracellular and intracellular concentration patterns, showed stronger activities related to arginine and methionine metabolism in CHL-YN than in CHO-K1. With the support of gene expression analysis of flask-batch host CHL-YN cells, we identified upregulated gene expression of several associated enzymes, namely ARG-2, CBS, and CTH, in CHL-YN cells. ARG-2 reportedly produces ornithine for purposes other than the urea cycle, such as polyamines, proline, and glutamate in mice (Deignan et al., 2006). Meanwhile, methyltransferases, CBS, and CTH are reportedly important enzymes for cysteine production (Chen & Betenbaugh, 2023). These findings suggest that CHL-YN cells have the potential to produce ornithine and cystathionine, resulting in proline and cysteine production. Furthermore, ornithine is also linked to metabolites in various pathways, including α -ketoglutarate, glutamate, and putrescine. Because it lacks arginase function, putrescine is a polyamine that reportedly serves as a growth-supportive supplement for CHO-K1 cells (Roca et al., 2019). Cystathionine is a precursor of cysteine production. Cysteine could then serve as a resource for glutathione biosynthesis, which responds to the generation of cellular reactive oxygen species and is correlated with mAb production performance (Chevallier et al., 2020). Therefore, these results suggest that CHL-YN cells had different capabilities not only in glutamine production, but also in ornithine and cystathionine production, confirming the reported dysfunction of related enzymes in CHO-K1 cells (Hefzi et al., 2016). However, high glutathione biosynthetic ability in CHL-YN cells could not prevent a drop in viability during the glutamine production phase. One of the possible causes of this was insufficient cysteine and glutathione production levels in CHL-YN cells to survive during this phase, which is associated with high cellular pressures such as amino acid depletion, toxic byproduct accumulation, and ammonium uptake. A case study on overexpressed CBS and CTH in CHO-GS cells reported the importance of methyltransferase (Chen & Betenbaugh, 2023). CHL-YN cells have strong gene expression of CBS and CTH, but not glycine N-methyltransferase (GNMT) like CHO-GS and CHO-K1 cells.

FIGURE 6 Concentrations of extracellular and intracellular metabolites in four phases of cell growth in the cell pool and B-08 clone of Chinese hamster lung (CHL)-YN-immunoglobulin G (IgG1) cells and the Chinese hamster ovary (CHO)-K1-IgG1 cell pool. Bar charts of prominent metabolites at four phases of cell growth in culture. (a) Four deprived amino acids. (b) Arginine-related metabolites, including the urea cycle and glutamate, proline, and polyamine biosynthesis. (c) Methionine-related metabolites, including the methionine cycle and cysteine biosynthesis. Area, relative area ratio; Ear, early exponential phase (Day 2 of CHL-YN and CHO-K1 cultures); Exp, middle exponential phase (Day 3 of CHL-YN and Day 4 of CHO-K1 cultures); Sta, stationary phase (Day 4 of CHL-YN and Day 6 of CHO-K1 cultures); and Del, decline phase (Day 5 of CHL-YN and Day 8 of CHO-K1 cultures).

Arginine metabolism (urea cycle, glutamate, proline, and polyamine biosynthesis)

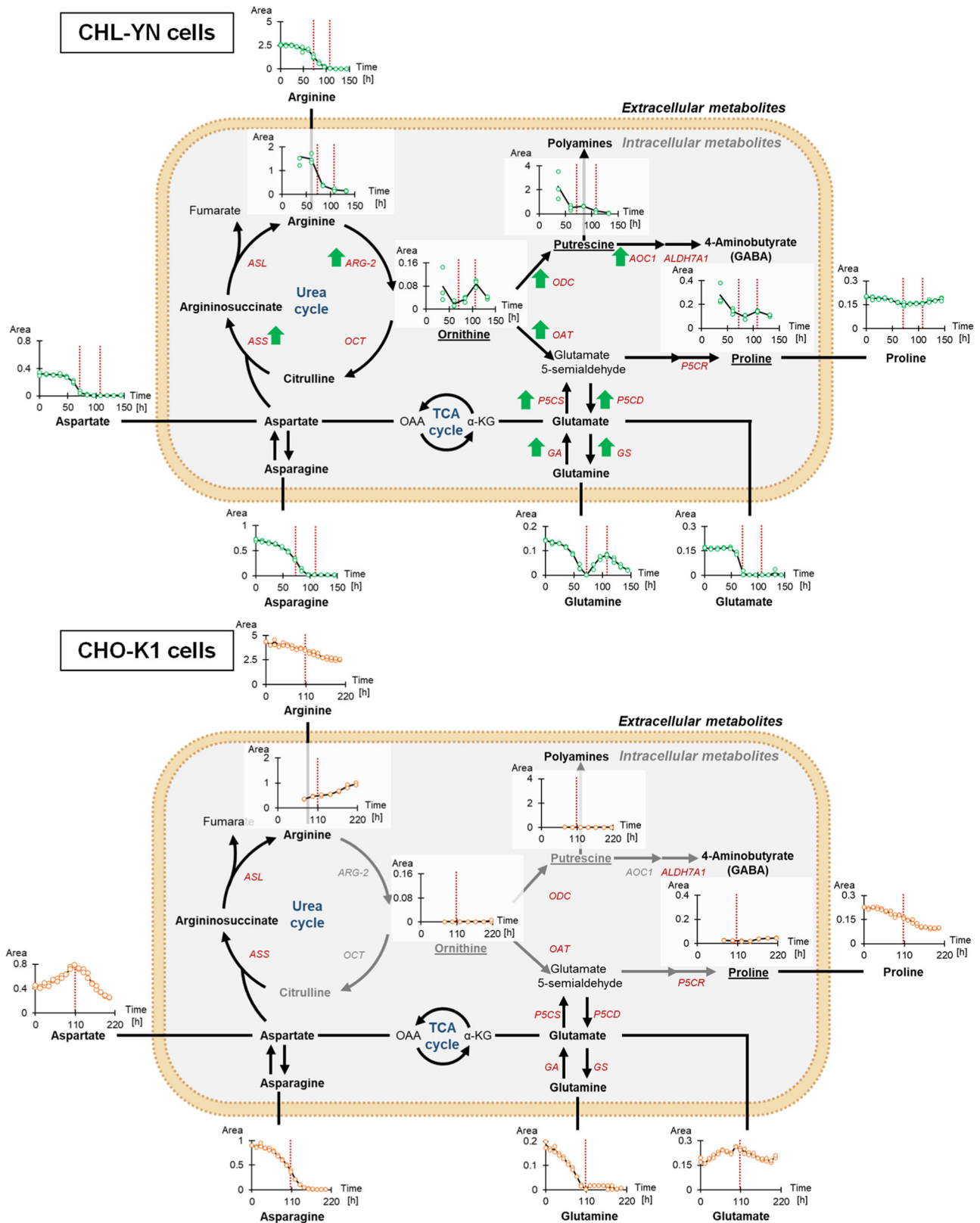


FIGURE 7 (See caption on next page).

Therefore, CHL-YN cells might utilize serine, instead of glycine, as a co-substrate to produce cysteine. When serine was nearly depleted, cysteine production would be stopped. Moreover, transcriptomic results showed that CTH gene expression was strongly reduced during this phase, leading to cystathionine accumulation. Nevertheless, since a drop in viability could occur due to several causes, it was suggested that further study focusing on the cell death of CHL-YN cells, such as apoptosis and autophagy, during glutamine production is warranted.

Intracellular metabolomics was performed via CE-MS-based targeted metabolomics, which offers efficient hydrophilic and ionic metabolite detection capability (Zhang & Ramautar, 2021), aimed to investigate further metabolites such as glycolysis intermediates. However, prominent information was not discovered. Finally, LC-MS/MS analysis of flask-batch cultures confirmed the differences in arginine and methionine metabolism between CHL-YN-IgG1 and CHO-K1-IgG1 cells.

Taken together, the results of this study uncovered the unique characteristics of glucose and glutamine metabolism in CHL-YN cells. Glucose consumption in CHL-YN cells exhibited a ~12 h-delayed shift and oscillated following glutamine metabolism, which was divided into three active phases: consumption (Days 1–3), production (Days 3.5–5.5), and re-consumption (Days 5.5–8). During the early growth phase (Days 1–3), glucose and glutamine were both consumed as carbon sources supporting cell growth. Although CHL-YN cells demanded glutamine at a higher level than CHO-K1 cells, both CHL-YN and CHO-K1 cells required glucose over glutamine based on the specific consumption rates. Glucose was utilized for ATP generation through glycolysis or was supplied to the pentose phosphate pathway. Meanwhile, glutamine was also taken up at a high level to replenish the α -ketoglutarate, an intermediate of the tricarboxylic acid (TCA) cycle (Coulet et al., 2022).

During depletion of extracellular glutamine (Day 3), the metabolism of CHL-YN cells shifted, and the glutamine production phase was started (Days 3.5–5.5). Glutamine production was higher in CHL-YN cells than in CHO-K1 cells because of the previously reported difference in glutamine synthetase expression (Yamano-Adachi et al., 2020). Strong glutamine synthetase activity could lead to an excessive level of glutamine production, which was demonstrated in CHO cells transfected with a synthetase expression system (Sacco et al., 2022). During glutamine production, extracellular glutamate

and ammonia are taken up into CHL-YN cells as a substrate, as shown in several cell lines, such as HEK293 (Lie et al., 2019). Furthermore, arginine metabolic activity may also be a source of glutamate, resulting in high glutamine production in CHL-YN cells.

Apart from arginine and methionine, several other amino acids (aspartate, isoleucine, leucine, phenylalanine, serine, tyrosine, and valine) were sharply consumed by CHL-YN cell cultures. These results suggest that, during glutamine production, these amino acids might be used for cellular activities or production of cellular components. Reductions in the levels of these amino acids also might have resulted from anaplerotic reactions, which have been observed in CHO cell cultures during entry to the stationary phase and serve to compensate for TCA cycle intermediates (Coulet et al., 2022). Intriguingly, phenylalanine, tyrosine, and branched chain amino acids (isoleucine, leucine, and valine) are reportedly sources of several cell-growth inhibitor byproducts (Coulet et al., 2022; Mulukutla et al., 2019). Thus, usage of these amino acids may be another explanation for the reduction in cell viability. Four amino acids were nearly depleted in our CHL-YN cultures: arginine, methionine, serine, and aspartate. A study using glutamine synthetase-expressing CHO cell cultures reported that serine was a limiting amino acid, while aspartate unavailability was a consequence of the limitation in asparagine (Duarte et al., 2014). Serine is thought to support methylation (Maddocks et al., 2016), while aspartate serves to replenish the TCA cycle, especially under low-glutamine conditions (Kirsch et al., 2022). In this study, we reported the critical importance of two new amino acids in fed-batch culture—arginine and methionine—that might be used for ornithine and cystathionine production.

Additionally, we observed that the availability of lactate switching in the stationary phase of CHL-YN-IgG1 cells resembled that found in cultivation of CHO cells (Hartley et al., 2018; Zagari et al., 2013). Although this phenomenon was also observed in CHO-K1 cells, CHL-YN cells had a lower calculated rate of glucose consumption. Meanwhile, the lactate consumption rate was higher in CHL-YN cells than in CHO-K1 cells (Supporting Information S2: Table 3). It is possible that the higher level of pyruvate replenishment from lactate causes CHL-YN cells to consume glucose more slowly than CHO-K1 cells, and might be related to the dramatic drop in glucose consumption of CHL-YN cells during the glutamine production phase.

FIGURE 7 Hypothesized model of differences in arginine metabolism between Chinese hamster lung (CHL)-YN and Chinese hamster ovary (CHO)-K1 cells. Hypothesized model of arginine metabolism, based on flask-batch extracellular and intracellular metabolomics and gene expression analyses, comparing the urea cycle and glutamate, proline, and polyamine biosynthesis activities in CHL-YN cells and CHO-K1 cells. Bolded metabolites were measured for extracellular and/or intracellular metabolomics; gray items represent undetected metabolites and mRNAs encoding the indicated enzymes; red items represent detected mRNAs encoding the indicated enzymes; black arrows indicate the activity of enzymes shown in red; gray arrows indicate the inactivity of the reaction; green arrows indicate >1.0 values of \log_2 (fold change) between CHL-YN (exponential) and CHO-K1 (exponential); red dotted lines in metabolic plots represent day 3 (72 h) and Days 5.5 (108 h) in the IgG1-producing cell pools of both CHL-YN and CHO-K1. Full names of the associated genes are provided in Supporting Information S2: Table 2. All time-course measurements of the relative area ratio (area) illustrating metabolite concentrations are shown in Supporting information S2: Figures 5 and 6.

Methionine metabolism (methionine cycle, cysteine and glutathione biosynthesis)

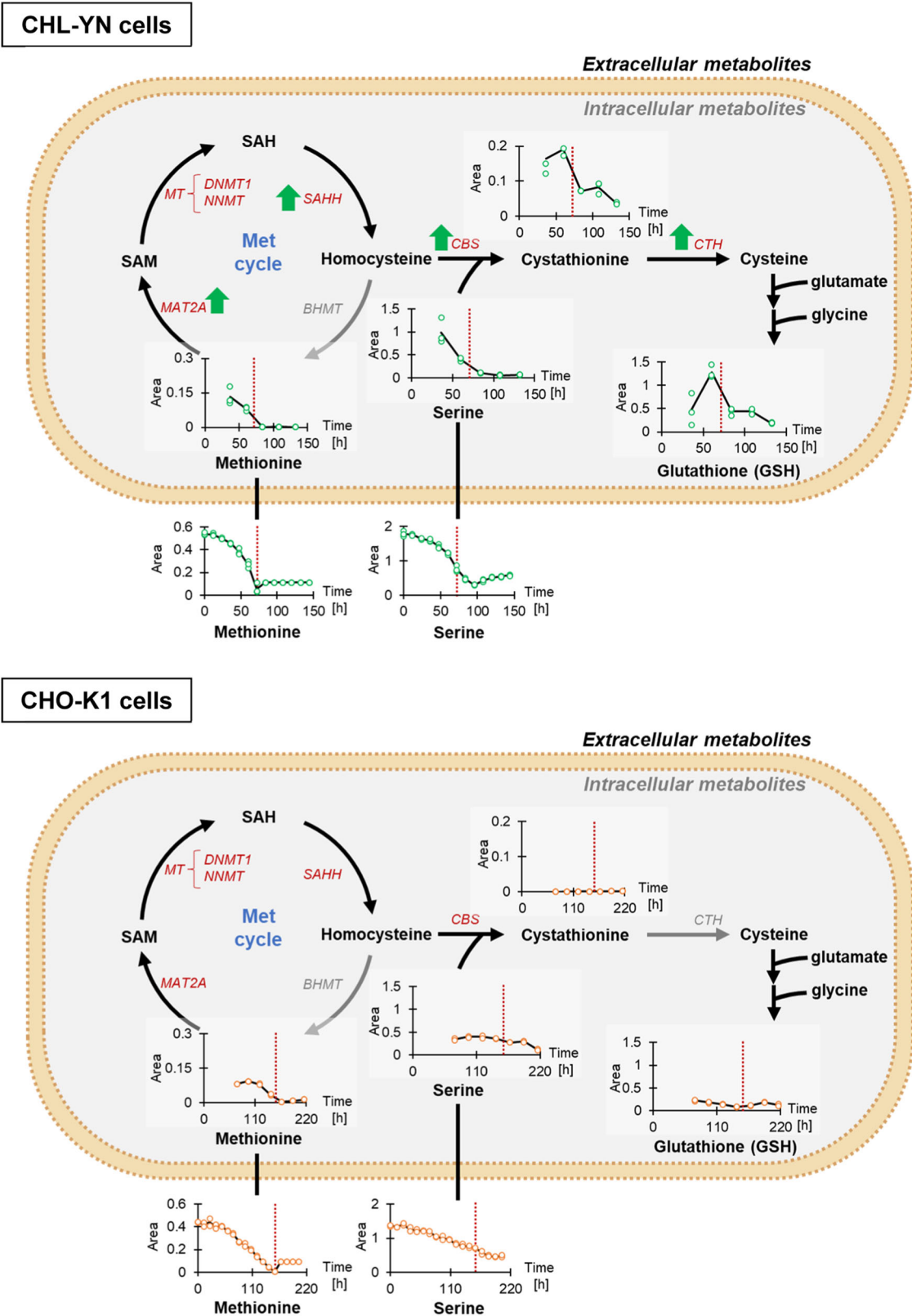


FIGURE 8 (See caption on next page).

The glutamine re-consumption phase observed in CHL-YN cultures (Days 5.5–8) did not occur in CHO-K1 cells, and may be attributable to the strong glutamine production phase in CHL-YN cells. Based on the metabolomics analysis of flask-batch cultivations, arginine depletion may be a driver of the second glutamine shift. The limited metabolic information and lack of data on biomass composition made it difficult to draw conclusions about our observations of apparent metabolic flux in this study. To better understand this phenomenon, we propose CHL-YN model construction and flux balance analysis as a future study.

In terms of antibody productivity on metabolic profiles, CHL-YN cells produced IgG in accordance with glutamine metabolism as well as glucose consumption patterns. IgG productivity was shown to be at the highest rates in the glutamine consumption phase, which has sufficient glucose, glutamine, and amino acid sources for both cell biosynthesis and IgG production. After that, the productivity dropped during the glutamine production phase. This stage has low glucose consumption and glutamine replenishment from other amino acids, leading to limited energy and amino acid sources for antibody production. Thus, glutamine production activity in CHL-YN cells may not be beneficial for IgG production. Then, IgG productivity was slightly increased during the glutamine re-consumption phase. This may have been due to the reversion of glucose, glutamine, and amino acid utilization during this stage. In view of this, we suggest that perfusion cultivation development for maintaining CHL-YN cell cultures in the glutamine consumption stage may be an efficient method to achieve high-volume IgG production. We also compared metabolic information between the CHL-YN cell pool and a high-IgG-producing clone, B-08, with the aim of discovering components critical for IgG production. However, the target metabolomic results in this study did not present differences in metabolic data sets. We suggest that a study comparing metabolic backgrounds between high- and low-IgG-producing CHL-YN clones may efficiently identify such components.

To further develop our CHL-YN fed-batch culture system for competitive, industrial-scale production, arginine and methionine feed optimization may be required to prolong cell viability and resulting in increased mAb production. Genetic engineering of CHL-YN cells could also be applied to improve mAb production performance. For instance, the nonantibiotic system dihydrofolate reductase (DHFR) selection system reportedly offers high gene amplification (Yang et al., 2022). Additionally, in CHL-YN

cells, gene modification of pathways related to arginine and methionine metabolism, with the aim of reducing metabolic depletion or overaccumulation, may improve mAb productivity. For example, overexpression of ornithine carbamoyl transferase in CHL-YN cells may facilitate arginine biosynthesis. Alternatively, downregulation of glutamine synthetase could be used to reduce glutamine secretion and increase mAb production, as shown in CHO-GS cells (Sacco et al., 2022). Similarly, modification of methionine cycle and transsulfuration pathway genes may be a further strategy to improve cysteine CHL-YN cell culture performance during the glutamine production phase and prevent the drop in viability under oxidative stress conditions (Chen & Betenbaugh, 2023).

In summary, we established a glucose feed control system for IgG1-producing CHL-YN cells. Using metabolomics analysis of CHL-YN and CHO-K1 cells, we discovered notable distinguishing features of CHL-YN beyond high glutamine synthesis, including a drop in glucose demand during the glutamine production phase, and proline and cysteine prototrophic abilities exerted through arginine and methionine metabolism.

AUTHOR CONTRIBUTIONS

Puriwat Sukwattanipaatt: Writing—original draft; writing—review and editing; conceptualization; methodology; and investigation. **Hirota Kuroda:** Writing—review and editing; methodology; and investigation. **Noriko Yamano-Adachi:** Writing—review and editing; conceptualization; supervision; and funding acquisition. **Takeshi Omasa:** Writing—review and editing; conceptualization; supervision; and funding acquisition.

ACKNOWLEDGMENTS

We appreciate Dr. Hiroaki Yamanaka, Mr. Kazumasa Kimura, and Mr. Wataru Kobayashi from Yokogawa Electric Corporation for supporting the bioreactor work and designing glucose feeding strategies. We also thank Michelle Kahmeyer-Gabbe, PhD, from Edanz (<https://jp.edanz.com/ac>) for editing a draft of this manuscript. This research was financially supported by the Japan Agency for Medical Research and Development (AMED) under Grant Numbers JP18ae0101066 and JP21ae0121021; the Japan Society for the Promotion of Science (JSPS) under KAKENHI Grant Number JP21K04788 and JP22H00276; and the Nikki/Saneyoshi Scholarship and Kinoshita Memorial Foundation Scholarship Program.

FIGURE 8 Hypothesized model of differences in methionine metabolism between Chinese hamster lung (CHL)-YN and Chinese hamster ovary (CHO)-K1 cells. Hypothesized model of methionine (Met) metabolism, based on flask-batch extracellular and intracellular metabolomics and gene expression analyses, comparing the Met cycle, cysteine, and glutathione biosynthesis activities in CHL-YN cells and CHO-K1 cells. Bolded metabolites were measured for extracellular and/or intracellular metabolomics; gray items represent undetected metabolites and mRNAs encoding the indicated enzymes; red items represent detected mRNAs encoding the indicated enzymes; black arrows indicate the activity of enzymes shown in red; gray arrows indicate the inactivity of the reaction; green arrows indicate >1.0 values of \log_2 (fold change) between CHL-YN (exponential) and CHO-K1 (exponential); red-dotted lines in metabolic plots represent day 3 (72 h) in the CHL-YN cell model and Day 6.5 (156 h) in the CHO-K1 cell model. Full names of the associated genes are provided in Supporting Information S2: Table 2. All time-course measurements of relative area ratio (area) illustrating metabolite concentrations are shown in Supporting information S2: Figures 5 and 6.

CONFLICT OF INTEREST STATEMENT

The authors declare no conflict of interest.

DATA AVAILABILITY STATEMENT

The data that support the findings of this study are available from the corresponding author upon reasonable request.

ORCID

Puriwat Sukwattananipaatt  <http://orcid.org/0000-0003-1767-8179>

Hirota Kuroda  <http://orcid.org/0009-0000-2473-7240>

Noriko Yamano-Adachi  <http://orcid.org/0000-0002-2167-5379>

Takeshi Omasa  <http://orcid.org/0000-0003-0635-3862>

REFERENCES

- Agrawal, V., & Bal, M. (2012). Strategies for rapid production of therapeutic proteins in mammalian cells. *BioProcess International*, 10(4), 32–48.
- Alhuthali, S., Kotidis, P., & Kontoravdi, C. (2021). Osmolality effects on CHO cell growth, cell volume, antibody productivity and glycosylation. *International Journal of Molecular Sciences*, 22(7), 3290. <https://doi.org/10.3390/ijms22073290>
- Badsha, M. B., Kurata, H., Onitsuka, M., Oga, T., & Omasa, T. (2016). Metabolic analysis of antibody producing Chinese hamster ovary cell culture under different stresses conditions. *Journal of Bioscience and Bioengineering*, 122(1), 117–124. <https://doi.org/10.1016/j.jbiosc.2015.12.013>
- Berting, A., Farcet, M. R., & Kreil, T. R. (2010). Virus susceptibility of Chinese hamster ovary (CHO) cells and detection of viral contaminations by adventitious agent testing. *Biotechnology and Bioengineering*, 106(4), 598–607. <https://doi.org/10.1002/bit.22723>
- Capella Roca, B., Lao, N., Barron, N., Doolan, P., & Clynes, M. (2019). An arginase-based system for selection of transfected CHO cells without the use of toxic chemicals. *Journal of Biological Chemistry*, 294(49), 18756–18768. <https://doi.org/10.1074/jbc.RA119.011162>
- Chen, Y., & Betenbaugh, M. J. (2023). Reconstruction of reverse transsulfuration pathway enables cysteine biosynthesis and enhances resilience to oxidative stress in Chinese Hamster Ovary cells. *Metabolic Engineering*, 76, 204–214. <https://doi.org/10.1016/j.ymben.2023.02.010>
- Chevallier, V., Schoof, E. M., Malphettes, L., Andersen, M. R., & Workman, C. T. (2020). Characterization of glutathione proteome in CHO cells and its relationship with productivity and cholesterol synthesis. *Biotechnology and Bioengineering*, 117(11), 3448–3458. <https://doi.org/10.1002/bit.27495>
- Chong, W. P. K., Thng, S. H., Hiu, A. P., Lee, D. Y., Chan, E. C. Y., & Ho, Y. S. (2012). LC-MS-based metabolic characterization of high monoclonal antibody-producing Chinese hamster ovary cells. *Biotechnology and Bioengineering*, 109(12), 3103–3111. <https://doi.org/10.1002/bit.24580>
- Coulet, M., Kepp, O., Kroemer, G., & Basmaciogullari, S. (2022). Metabolic profiling of CHO cells during the production of biotherapeutics. *Cells*, 11(12), 1929. <https://doi.org/10.3390/cells11121929>
- Čuperlović-Culf, M., Barnett, D. A., Culf, A. S., & Chute, I. (2010). Cell culture metabolomics: Applications and future directions. *Drug Discovery Today*, 15(15–16), 610–621. <https://doi.org/10.1016/j.drudis.2010.06.012>
- Deignan, J., Livesay, J., Yoo, P., Goodman, S., OBRIEN, W., Iyer, R., Cederbaum, S., & Grody, W. (2006). Ornithine deficiency in the arginase double knockout mouse. *Molecular Genetics and Metabolism*, 89(1–2), 87–96. <https://doi.org/10.1016/j.ymgme.2006.04.007>
- Duarte, T. M., Carinhas, N., Barreiro, L. C., Carrondo, M. J. T., Alves, P. M., & Teixeira, A. P. (2014). Metabolic responses of CHO cells to limitation of key amino acids. *Biotechnology and Bioengineering*, 111(10), 2095–2106. <https://doi.org/10.1002/bit.25266>
- Fan, Y., Ley, D., & Andersen, M. R. (2018). Fed-batch CHO cell culture for lab-scale antibody production. *Methods in Molecular Biology*, 1674, 147–161. https://doi.org/10.1007/978-1-4939-7312-5_12
- Hartley, F., Walker, T., Chung, V., & Morten, K. (2018). Mechanisms driving the lactate switch in Chinese hamster ovary cells. *Biotechnology and Bioengineering*, 115(8), 1890–1903. <https://doi.org/10.1002/bit.26603>
- Hefzi, H., Ang, K. S., Hanscho, M., Bordbar, A., Ruckerbauer, D., Lakshmanan, M., Orellana, C. A., Baycin-Hizal, D., Huang, Y., Ley, D., Martinez, V. S., Kyriakopoulos, S., Jiménez, N. E., Zielinski, D. C., Quek, L. E., Wulff, T., Arnsdorf, J., Li, S., Lee, J. S., ... Lewis, N. E. (2016). A consensus genome-scale reconstruction of Chinese hamster ovary cell metabolism. *Cell Systems*, 3(5), 434–443.e8. <https://doi.org/10.1016/j.cels.2016.10.020>
- Horie, M., Yamano-Adachi, N., Kawabe, Y., Kaneoka, H., Fujita, H., Nagamori, E., Iwai, R., Sato, Y., Kanie, K., Ohta, S., Somiya, M., & Ino, K. (2022). Recent advances in animal cell technologies for industrial and medical applications. *Journal of Bioscience and Bioengineering*, 133(6), 509–514. <https://doi.org/10.1016/j.jbiosc.2022.03.005>
- Horiuchi, T. (2019). Establishment of a novel CHO cell line and its application to the production of protein-based pharmaceuticals. *Seibutsu-kogaku Kaishi (in Japanese)*, 97, 328–330.
- Kawabe, Y., & Kamihira, M. (2022). Novel cell lines derived from Chinese hamster kidney tissue. *PLoS One*, 17(3 March), 0266061. <https://doi.org/10.1371/journal.pone.0266061>
- Kirsch, B. J., Bennun, S. V., Mendez, A., Johnson, A. S., Wang, H., Qiu, H., Li, N., Lawrence, S. M., Bak, H., & Betenbaugh, M. J. (2022). Metabolic analysis of the asparagine and glutamine dynamics in an industrial Chinese hamster ovary fed-batch process. *Biotechnology and Bioengineering*, 119(3), 807–819. <https://doi.org/10.1002/bit.27993>
- Kunert, R., & Reinhart, D. (2016). Advances in recombinant antibody manufacturing. *Applied Microbiology and Biotechnology*, 100(8), 3451–3461. <https://doi.org/10.1007/s00253-016-7388-9>
- Lee, T. Y., Lin, H. H., Chen, C. L., Hwang, S. M., & Tseng, C. P. (2015). Inhibitory effect of excessive glucose on its biochemical pathway and the growth of Chinese hamster ovary (CHO) cells. *Journal of Carbohydrate Chemistry*, 34(1), 1–11. <https://doi.org/10.1080/07328303.2014.977908>
- Lie, S., Wang, T., Forbes, B., Proud, C. G., & Petersen, J. (2019). The ability to utilise ammonia as nitrogen source is cell type specific and intricately linked to GDH, AMPK and mTORC1. *Scientific Reports*, 9(1), 1461. <https://doi.org/10.1038/s41598-018-37509-3>
- Lu, R. M., Hwang, Y. C., Liu, I. J., Lee, C. C., Tsai, H. Z., Li, H. J., & Wu, H. C. (2020). Development of therapeutic antibodies for the treatment of diseases. *Journal of Biomedical Science*, 27(1), 1–30. <https://doi.org/10.1186/s12929-019-0592-z>
- Maddocks, O. D. K., Labuschagne, C. F., Adams, P. D., & Vousden, K. H. (2016). Serine metabolism supports the methionine cycle and DNA/RNA methylation through de novo ATP synthesis in cancer cells. *Molecular Cell*, 61(2), 210–221. <https://doi.org/10.1016/j.molcel.2015.12.014>
- Mulukutla, B. C., Mitchell, J., Geoffroy, P., Harrington, C., Krishnan, M., Kalomeris, T., Morris, C., Zhang, L., Pegman, P., & Hiller, G. W. (2019). Metabolic engineering of Chinese hamster ovary cells towards reduced biosynthesis and accumulation of novel growth inhibitors in fed-batch cultures. *Metabolic Engineering*, 54, 54–68. <https://doi.org/10.1016/j.ymben.2019.03.001>
- Okamura, K., Badr, S., Murakami, S., & Sugiyama, H. (2022). Hybrid modeling of CHO cell cultivation in monoclonal antibody production with an impurity generation module. *Industrial & Engineering*

- Chemistry Research*, 61(40), 14898–14909. <https://doi.org/10.1021/acs.iecr.2c00736>
- Omasa, T., Higashiyama, K. I., Shioya, S., & Suga, K. (1992). Effects of lactate concentration on hybridoma culture in lactate-controlled fed-batch operation. *Biotechnology and Bioengineering*, 39(5), 556–564. <https://doi.org/10.1002/bit.260390511>
- Omasa, T., Onitsuka, M., & Kim, W. D. (2010). Cell engineering and cultivation of Chinese hamster ovary (CHO) cells. *Current Pharmaceutical Biotechnology*, 11(3), 233–240. <https://doi.org/10.2174/138920110791111960>
- Pereira, S., Kildegaard, H. F., & Andersen, M. R. (2018). Impact of CHO metabolism on cell growth and protein production: An overview of toxic and inhibiting metabolites and nutrients. *Biotechnology Journal*, 13(3), e1700499. <https://doi.org/10.1002/biot.201700499>
- Poulain, A., Mullick, A., Massie, B., & Durocher, Y. (2019). Reducing recombinant protein expression during CHO pool selection enhances frequency of high-producing cells. *Journal of Biotechnology*, 296(March), 32–41. <https://doi.org/10.1016/j.jbiotec.2019.03.009>
- Puck, T. T., Cieciura, S. J., & Robinson, A. (1958). Genetics of somatic mammalian cells. *The Journal of Experimental Medicine*, 108(77), 945–956. <https://doi.org/10.1084/jem.108.6.945>
- Ritacco, F. V., Wu, Y., & Khetan, A. (2018). Cell culture media for recombinant protein expression in Chinese hamster ovary (CHO) cells: History, key components, and optimization strategies. *Biotechnology Progress*, 34(6), 1407–1426. <https://doi.org/10.1002/btpr.2706>
- Sacco, S. A., Tuckowski, A. M., Trenary, I., Kraft, L., Betenbaugh, M. J., Young, J. D., & Smith, K. D. (2022). Attenuation of glutamine synthetase selection marker improves product titer and reduces glutamine overflow in Chinese hamster ovary cells. *Biotechnology and Bioengineering*, 119(7), 1712–1727. <https://doi.org/10.1002/bit.28084>
- Sakaki, A., Namatame, T., Nakaya, M., & Omasa, T. (2023). Model-based control system design to manage process parameters in mammalian cell culture for biopharmaceutical manufacturing. *Biotechnology and Bioengineering*, 121(2), 605–617. <https://doi.org/10.1002/bit.28593>
- Schulze, M., Niemann, J., Wijffels, R. H., Matuszczyk, J., & Martens, D. E. (2022). Rapid intensification of an established CHO cell fed-batch process. *Biotechnology Progress*, 38(1), 1–15. <https://doi.org/10.1002/btpr.3213>
- Stepper, L., Filser, F. A., Fischer, S., Schaub, J., Gorr, I., & Voges, R. (2020). Pre-stage perfusion and ultra-high seeding cell density in CHO fed-batch culture: A case study for process intensification guided by systems biotechnology. *Bioprocess and Biosystems Engineering*, 43(8), 1431–1443. <https://doi.org/10.1007/s00449-020-02337-1>
- Stolfa, G., Smonskey, M. T., Boniface, R., Hachmann, A. B., Gulde, P., Joshi, A. D., Pierce, A. P., Jacobia, S. J., & Campbell, A. (2018). CHO-omics review: The impact of current and emerging technologies on Chinese hamster ovary based bioproduction. *Biotechnology Journal*, 13(3), e1700227. <https://doi.org/10.1002/biot.201700227>
- Tihanyi, B., & Nyitray, L. (2020). Recent advances in CHO cell line development for recombinant protein production. *Drug Discovery Today: Technologies*, 38, 25–34. <https://doi.org/10.1016/j.ddtec.2021.02.003>
- Vodopivec, M., Lah, L., Narat, M., & Curk, T. (2019). Metabolomic profiling of CHO fed-batch growth phases at 10, 100, and 1,000 L. *Biotechnology and Bioengineering*, 116(10), 2720–2729. <https://doi.org/10.1002/bit.27087>
- Walsh, G., & Walsh, E. (2022). Biopharmaceutical benchmarks 2022. *Nature Biotechnology*, 40(12), 1722–1760. <https://doi.org/10.1038/s41587-022-01582-x>
- Wurm, F. M., & Hacker, D. (2011). First CHO genome. *Nature Biotechnology*, 29(8), 718–720. <https://doi.org/10.1038/nbt.1943>
- Yamano-Adachi, N., Arishima, R., Puriwat, S., & Omasa, T. (2020). Establishment of fast-growing serum-free immortalised cells from Chinese hamster lung tissues for biopharmaceutical production. *Scientific Reports*, 10(1), 17612. <https://doi.org/10.1038/s41598-020-74735-0>
- Yang, W., Zhang, J., Xiao, Y., Li, W., & Wang, T. (2022). Screening strategies for high-yield Chinese hamster ovary cell clones. *Frontiers in Bioengineering and Biotechnology*, 10, 1–11. <https://doi.org/10.3389/fbioe.2022.858478>
- Zagari, F., Jordan, M., Stettler, M., Broly, H., & Wurm, F. M. (2013). Lactate metabolism shift in CHO cell culture: The role of mitochondrial oxidative activity. *New Biotechnology*, 30(2), 238–245. <https://doi.org/10.1016/j.nbt.2012.05.021>
- Zhang, W., & Ramautar, R. (2021). CE-MS for metabolomics: Developments and applications in the period 2018–2020. *Electrophoresis*, 42(4), 381–401. <https://doi.org/10.1002/elps.202000203>

SUPPORTING INFORMATION

Additional supporting information can be found online in the Supporting Information section at the end of this article.

How to cite this article: Sukwattananipaat, P., Kuroda, H., Yamano-Adachi, N., & Omasa, T. (2024). Metabolomic characterization of monoclonal antibody-producing Chinese hamster lung (CHL)-YN cells in glucose-controlled serum-free fed-batch operation. *Biotechnology and Bioengineering*, 1–20. <https://doi.org/10.1002/bit.28777>